ORNL-2812
UC-41 - Health and Safety

CALCULATION OF TEMPERATURE RISE IN DEEPLY BURIED RADIOACTIVE CYLINDERS

J. J. Perona
M. E. Whatley

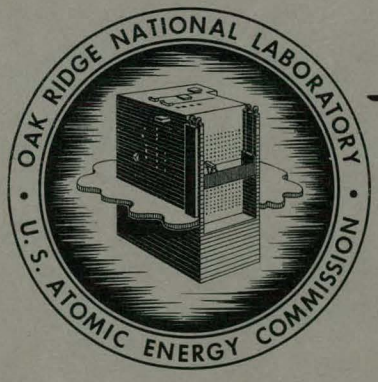

OAK RIDGE NATIONAL LABORATORY
operated by
UNION CARBIDE CORPORATION
for the
U.S. ATOMIC ENERGY COMMISSION

DISCLAIMER

Printed in USA. Price $1.25. Available from the
Office of Technical Services
Department of Commerce
Washington 25, D.C.

ORNL-2812

Contract No. W-7405-eng-26

Chemical Technology Division
Unit Operations Section

CALCULATION OF TEMPERATURE RISE IN DEEPLY BURIED RADIOACTIVE CYLINDERS

J. J. Perona
M. E. Whatley

DATE ISSUED

FEB 25 1960

OAK RIDGE NATIONAL LABORATORY
Oak Ridge, Tennessee
operated by
UNION CARBIDE CORPORATION
for the
U. S. Atomic Energy Commission

ABSTRACT

Temperatures were calculated, for application to the storage of radioactive solid waste, as a function of time and radial distance for radioactive solid cylinders in infinite solid media of "average soil," "average rock," and salt. A resistance at the cylinder—infinite medium boundary was included in the form of an air space.

For the range of parameters used and within the practical limits of accuracy, the maximum temperature rise increased linearly with the heat generation rate. The fission product spectrum was not significant in the determination of the maximum temperature rise. Under the pessimistic storage conditions assumed in this study, the storage of cylinders of a practical size appears feasible without excessive temperature rise. A maximum temperature rise of 1000°F would be produced with an initial heat generation rate of 1300-1600 Btu/hr·ft^3 for cylinders with a 5-in. radius, with 350-450 Btu/hr·ft^3 for a 10-in. radius, and with 175-210 Btu/hr·ft^3 for a 15-in. radius, assuming a thermal conductivity of the radioactive cylinder of 0.1 Btu/hr·ft·°F.

CONTENTS

1.0 INTRODUCTION

Herein are reported calculations of temperature rise in deeply buried radioactive cylinders. The emission and attenuation of beta and gamma rays within a radioactive solid results in the generation of heat which must either be stored in the solid as sensible heat or dissipated to the environment. The calculation of temperature rise in deeply buried radioactive solids has immediate application to the several programs on ultimate disposal of radioactive wastes as solids. Conditions of storage for such wastes must be such as to prevent temperature rise sufficiently high to cause evolution of gases or to threaten the structural integrity of the storage system. A criterion for safe storage would probably be to prevent the rise of temperatures above those reached during the calcination process. The maximum temperature rise in radioactive solid cylinders separated from an infinite solid medium by a 1-in. air space was calculated over a range of cavity radii of 5 to 30 in. with heat generation rates up to 2000 Btu/hr·ft^3. The assumed thermal conductivity of the radioactive cylinders was varied from 0.1 to 1.0 Btu/hr·ft·°F.

Cylindrical geometry for the radioactive solid was chosen because the cylinders can be sufficiently small in diameter to prevent excessive temperature rise but sufficiently long to permit storage of a large amount of material. Furthermore, cylindrical cavities can be conveniently made by drilling. Conditions of storage of radioactive solid cylinders in infinite solid media of "average soil," "average rock," and salt were investigated. The effects of specific heat generation rate, fission product spectrum, thermal conductivity of the radioactive cylinder, and convection coefficient in the air space were studied.

The advantages in the conversion of liquid wastes to solids prior to storage are decreased mobility and corrosion and either fixation of fission products or volume reduction. Fixation of fission products into a glass or clay matrix in a nonleachable form generally precludes a significant volume decrease. The problem of temperature rise is usually made worse by the conversion from liquid to solid in that the specific heat generation rate is increased in proportion to the volume decrease and the mechanism of convection is no longer available for heat dissipation. Three general methods of liquid to solid conversion are being developed currently: (a) evaporation to dryness followed by thermal decomposition (calcination) in the range 400-800°C,[1-4] (b) formation of a gel by the addition of mineral constituents with subsequent drying and firing at about 1200°C to form a glass,[5] and (c) sorption of fission products on clay followed by firing at about 1000°C.[6,7] The calcination method appears likely to produce solid wastes with the highest volumetric heat generation rates and lowest thermal conductivities.

Calculations for the storage of spherical and cylindrical shapes, with the physical properties of glass and diameters ranging from 0.25 to 2.0 ft, were made at Chalk River[8] for the condition of shallow burial of radioactive solids in sand. At burial depths of 10 ft, the heat of decay is soon dissipated to the atmosphere at the surface of the earth. Steady-state heat transfer was assumed in both the radioactive solid and the sand medium. Perring[9] of Harwell chose as his system an infinitely long cylinder of radioactive

solid in perfect thermal contact with an infinite solid medium of the same thermal conductivity. The assumption of "same thermal conductivity" greatly simplified analytical treatment. The physical properties of fire-brick at 500°C were used. Axial cylinder temperatures as a function of time were obtained for two fission product concentrations and cylinder diameters of 5, 10, and 20 cm. Rodger and Fineman[10] of Argonne National Laboratory used the solution for a constant continuous line source to approximate the temperature at the surface of a long, thin cylindrical cavity in an infinite solid medium. The temperature rise in a 2-ft-dia cylinder was calculated for a certain one-year cooled waste, assuming thermal conductivities of 0.1 and 0.5 Btu/hr.ft.°F for the radioactive solid and the surrounding earth, respectively.

Symbols. The following symbols are used in the equations:

A area, ft^2

c heat capacity, Btu/lb·°F

D diameter, ft

h convection coefficient, Btu/hr·ft^2·°F

k thermal conductivity, Btu/hr·ft^2 (°F/ft)

m $\dfrac{r_{i+1} - r_i}{r_i}$

q heat flux, Btu/hr·ft^2

q_o initial heat flux, Btu/hr·ft^2

Q heat generation rate, Btu/hr·ft^3

Q_o initial heat generation rate, Btu/hr·ft^3

r radial distance, ft

R radius of radioactive cylinder, ft

R_2 radius of cylindrical cavity, ft

t time, hr

T temperature, °F

T_A ambient temperature, °F

T_o initial temperature, °F

T_S surface temperature, °F

u variable of integration

α thermal diffusivity, $ft^2/hr = \frac{k}{\rho c}$

β a root of the equation: $\beta J_1(R\beta) = h/k\ J_o\ (R\beta)$

γ 0.57722 . . . = Euler's constant

ρ density, lb/ft^3

λ radioactive decay constant, hr^{-1}

2.0 STORAGE MODEL AND SUBSIDIARY EQUATIONS

The specific physical application which prompted this calculation is the storage of long cylindrical containers filled with calcined radioactive wastes in holes drilled in the earth, but the results of the calculation are somewhat more general. The problem involves diffusion of heat from a decaying uniform heat source through an air gap into an infinite solid medium in cylindrical geometry. The heat results from the decay of several fission products, and it decays as a composite of exponentials. An analytical solution, if derived, would be cumbersome to evaluate. The problem is more easily solved by the use of digital computer techniques. The complexity of the calculation is greatly decreased if certain simplifying assumptions can be made. To gain insight into the problem and to evaluate possible assumptions, some limiting cases were studied for which there are analytical solutions.

First, the temperature transients within the cylinder itself were studied using uniform initial temperature distribution, a uniform and constant heat source, and a constant temperature air sink. The results of this study showed that the steady-state temperature distribution within the cylinder could be assumed both as an initial condition and throughout the storage calculation.

Secondly, the limiting case of a constant heat flux at the surface of a cylindrical cavity in an infinite solid was studied. The complexity of this case was significant in pointing up the desirability of a numerical solution of the more complex problem of the decaying heat source. Results from this study were useful in establishing the convergence of the subsequent numerical calculation.

Finally, the problem of the decaying heat source in the infinite medium was divided into two parts, (a) the determination of the temperature rise in the surrounding medium by numerical calculation, and (b) the temperature drop through the cylindrical container of solids and the air space by analytical calculation (Fig. 1). The results of the first calculation can also be applied to the storage of cylindrical containers of liquid radioactive wastes, and the latter to the storage of radioactive solid cylinders in an isothermal medium. The calculation of storage of cylindrical containers of radioactive solids in an infinite medium without an air gap is not reported in this work, but can be easily computed from the calculations presented here.

UNCLASSIFIED
ORNL-LR-DWG 36419

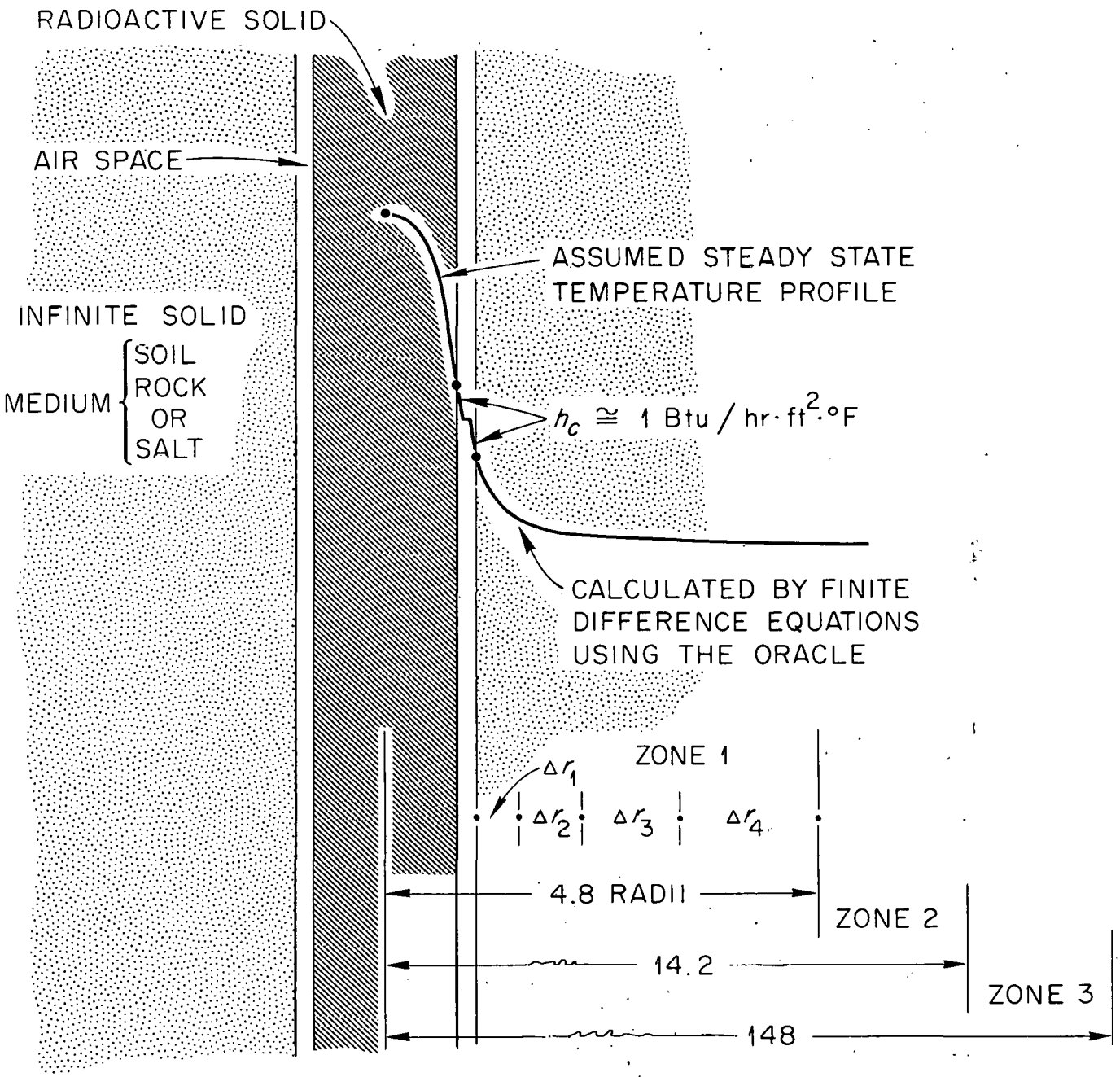

Fig. 1. Model for Calculations of Temperature Rise in a Cylinder of Radioactive Waste.

2.1 Temperatures in Solid Cylinders, Initially at Uniform Temperature, with Constant Heat Generation and Convection Cooling at the Surface

The history of a radioactive cylinder from the time of its formation to the time of storage is of interest since it fixes the initial condition for the storage calculation. At the time of its formation, a radioactive cylinder will probably be at a uniformly high temperature; for example, it may be formed by the calcination of a waste liquid. The equation of heat conduction for this case is

$$\frac{\partial^2 T}{\partial r^2} + \frac{1}{r}\frac{\partial T}{\partial r} + \frac{Q}{k} = \frac{1}{\alpha}\frac{\partial T}{\partial t} \tag{1}$$

with the initial condition

$$T = T_o \text{ at } t = 0 \tag{2}$$

and boundary conditions

$$\frac{\partial T}{\partial r} = 0 \text{ at } r = 0 \qquad -k\frac{\partial T}{\partial r} = hT \text{ at } r = R \tag{3,4}$$

This set of equations can be reduced to a set with known solutions by assuming

$$T(r,t) = T_1(r,t) + T_2(r) \tag{5}$$

Equation 1 now becomes

$$\frac{\partial^2 T_1}{\partial r^2} + \frac{\partial T_2}{\partial r^2} + \frac{1}{r}\left(\frac{\partial T_1}{\partial r} + \frac{\partial T_2}{\partial r}\right) + \frac{Q}{k} = \frac{1}{\alpha}\frac{\partial T_1}{\partial t} \tag{6}$$

with the initial condition

$$T_1 + T_2 = T_o \text{ at } t = 0 \tag{7}$$

and boundary conditions

$$\frac{\partial T_1}{\partial r} = 0 \text{ and } \frac{\partial T_2}{\partial r} = 0 \text{ at } r = 0 \tag{8}$$

$$-k\frac{\partial T_1}{\partial r} = hT_1 \text{ at } r = R \tag{9}$$

$$-k\frac{\partial T_2}{\partial r} = hT_2 \text{ at } r = R \tag{10}$$

Separating variables in eq. 6 yields

$$\frac{\partial^2 T_1}{\partial r^2} + \frac{1}{r}\frac{\partial T_1}{\partial r} = \frac{1}{\alpha}\frac{\partial T_1}{\partial t} \tag{11}$$

$$\frac{\partial^2 T_2}{\partial r^2} + \frac{1}{r}\frac{\partial T_2}{\partial r} + \frac{Q}{k} = 0 \tag{12}$$

Equation 11 with conditions 7, 8, and 9 has been solved by Carslaw and Jaeger:[11]

$$T_1 = \frac{2h(T_o - T_2)}{kR} \sum_{n=1}^{\infty} e^{-\alpha\beta_n^2 t} \frac{J_o(r\beta_n)}{\left(\frac{h^2}{k^2} + \beta_n^2\right) J_o(R\beta_n)} \tag{13}$$

where β_n are the roots of

$$\beta J_1(R\beta) = \frac{h}{k} J_o(R\beta) \tag{14}$$

The solution to eq. 12 with conditions 8 and 10 is

$$T_2 = \frac{QR^2}{4k}\left(1 - \frac{r^2}{R^2} + \frac{2k}{hR}\right) \tag{15}$$

Combining equations 13 and 15 yields the desired solution:

$$T = \frac{QR^2}{4k}\left(1 - \frac{r^2}{R^2} + \frac{2k}{hR}\right) + \frac{2h}{kR}\left[T_o - \frac{QR^2}{4k}\left(1 - \frac{r^2}{R^2} - \frac{2k}{hR}\right)\right] \sum_{n=1}^{\infty} \exp\left(-\alpha\beta_n^2 t\right) \frac{J_o(r\beta_n)}{\left(\frac{h^2}{k^2} + \beta_n^2\right) J_o(R\beta_n)} \tag{16}$$

at steady state ($t \rightarrow \infty$) and

$$T = \frac{QR^2}{4k}\left(1 - \frac{r^2}{R^2} + \frac{2k}{hR}\right) \tag{17}$$

Equation 16 was used to calculate the approach to steady state for

a few sample conditions of interest in waste processing. Assuming natural convection cooling with air, a convection coefficient of about 1 Btu/hr·ft^2·°F was estimated and checked[12] after calculation of surface temperatures by

$$h = 0.27\left(\frac{T_s - T_A}{D}\right)^{0.25} \tag{18}$$

For the case of natural convection cooling in water, a coefficient of 30 Btu/hr·ft^2·°F was estimated.[12] A thermal diffusivity of 0.006 ft^2/hr was assumed, based on values of Al_2O_3 of 0.0075 ft^2/hr and for Fe_2O_3 of 0.0059 ft^2/hr.[13] Assuming an initial uniform temperature of 1300°F, which might be reached in a calcining or fusing operation, the steady-state centerline temperature was approached within 10°F in 30 to 150 hr over the ranges of radii from 0.333 to 1.0 ft and thermal conductivities from 0.1 to 1.0 Btu/hr·ft·°F (Fig. 2a, b). On the basis of these calculations, the cylinders were assumed to have reached their steady-state temperature distributions prior to storage (refer to assumptions in Sec. 3.2).

Since the rate of heat generation by radioactive wastes discharged from the reactor one year or more would decrease less than 5% in one or two weeks, the assumption of "constant" heat generation rate during the unsteady-state period is permissible. After reaching an apparent steady state, the temperature distribution in the cylinder would decrease differentially as the heat generation rate continuously decreased as a result of radioactive decay. However, the temperature distribution in the cylinder can be calculated with good accuracy at any time by using the proper value of instantaneous heat generation rate in the steady-state equations.

2.2 Infinite Cylindrical Cavity in Infinite Medium with Constant Heat Flux at Boundary

This case was derived by Carslaw and Jaeger for zero initial temperature:[14]

$$T = -\frac{2Q}{\pi k}\int_0^\infty \left(1 - e^{-\alpha\mu^2 t}\right) \frac{J_0(\mu r)\, Y_1(\mu R_2) - Y_0(\mu r)\, J_1(\mu R_2)}{\mu^2\left[J_1^2(\mu R_2) + Y_1^2(\mu R_2)\right]}\, d\mu \tag{19}$$

Equation 19 is not in convenient form for numerical evaluation, but Carslaw and Jaeger present a graph for the evaluation of surface temperature for values of $\alpha t/R_2^2$ less than 10. For large values of time, the surface temperature is given by

$$T = \frac{QR_2}{2k}\left[\ln\left(\frac{4\alpha t}{R_2^2}\right) - \gamma\right] + O\left(\frac{R_2^2}{\alpha t}\right) \tag{20}$$

where $\gamma = 0.57722$ is Euler's constant and the Landau O indicates that the remainder term is of the order of $R_2^2/\alpha t$. For this case of constant

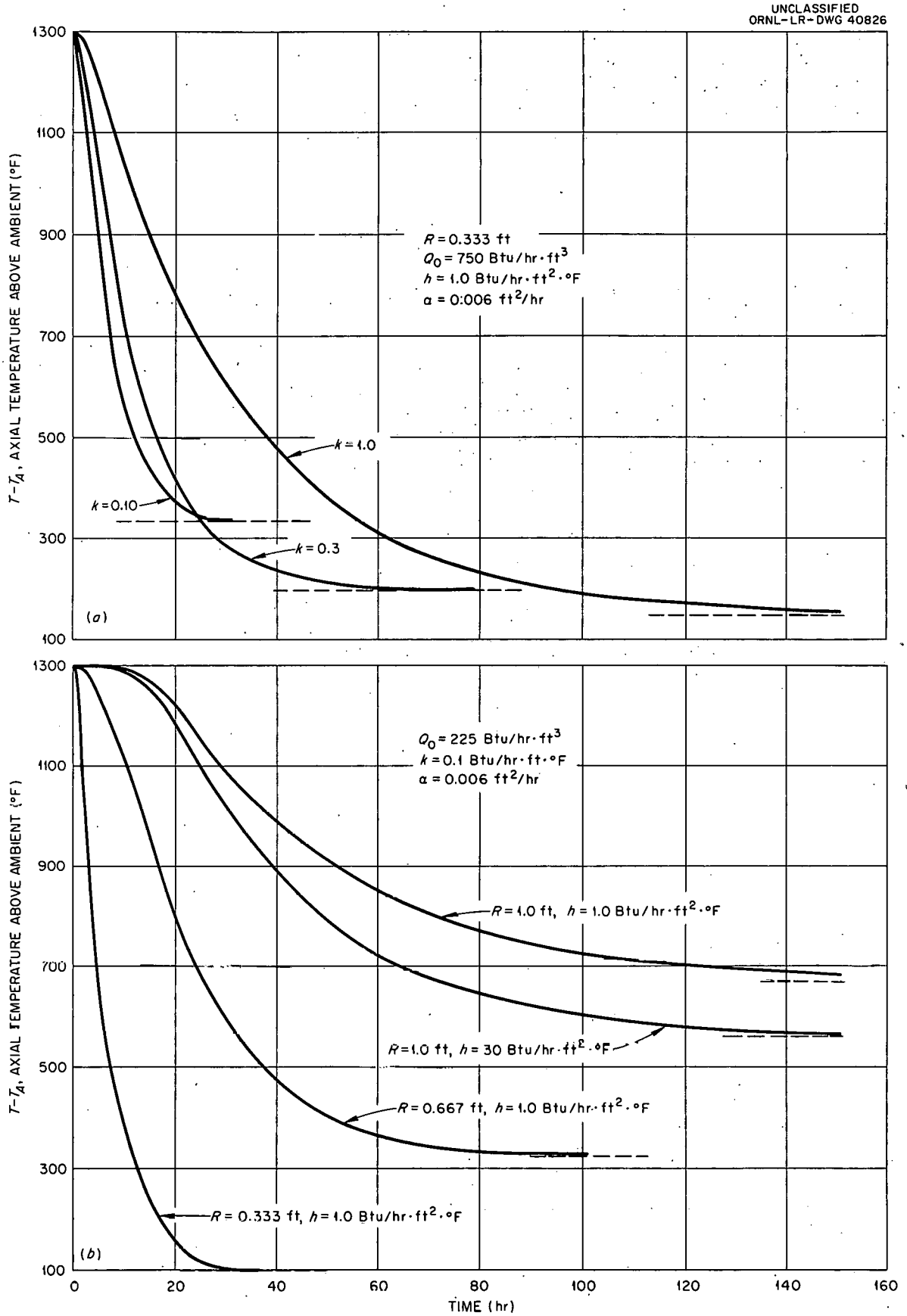

Fig. 2. Approach to Steady State for Infinite Cylinders of Radioactive Material, Showing Effect of (*a*) Thermal Conductivity and (*b*) Radius. Cylinder Initially at Uniform Temperature of 1300°F.

heat flux, eq. 20 shows that the surface temperature increases logarithmically without limit as the time increases. For the period of time in which $\alpha t/R_2^2$ is greater than 10 but the heat generation rate has not yet decreased appreciably, eq. 20 can be used to calculate the cavity surface temperature. It will be seen later that the period of time over which eq. 20 can be used is the period of greatest interest.

3.0 DECAYING HEAT FLUX CALCULATIONS AND STORAGE MODEL ASSUMPTIONS

3.1 An Infinite Cylindrical Cavity in an Infinite Medium with a Decaying Heat Flux at the Boundary

A solution for this case by the methods of classical mathematical physics would be even more complicated and cumbersome to evaluate than eq. 19. For this reason the decision was made to obtain numerical solutions for the cases of interest by a finite-difference method. Explicit difference equations were derived and a code utilizing them was written for the Oracle. The results of these calculations are presented in Sec. 5.1.

A detailed derivation of the difference equations is given in the appendix (Sec. 7.2). The equations, based on Fig. 3, are

$$T_{1,t+\Delta t} = \frac{qr_1}{kM_1}\ln(1+m) + \frac{(M_1 - 1)\,T_{1,t} + T_{2,t}}{M_1} \tag{21}$$

where

$$M_1 = \frac{r_1^2}{2\alpha\Delta t}\left[\frac{m^2}{\ln(1+m)} - \ln(1+m)\right] \tag{22}$$

and

$$T_{i,t+\Delta t} = \frac{T_{i-1,t} + (M_i - 2)\,T_{i,t} + T_{i+1,t}}{M_i} \quad (i = 2, 3, 4, \ldots, 15) \tag{23}$$

where

$$M_i = \frac{r_i^2 - 1}{2\alpha\Delta t}\left[\frac{m^3(2+m)}{\ln(1+m)}\right] \tag{24}$$

Necessary conditions for the stability of the difference equations are $M_1 > 1$ and $M_i > 2$. If the size of the assumed time increment is too large, errors introduced by approximations are amplified and eventually cause wildly oscillating temperatures to be calculated.[15] The solid medium was divided into increments increasing with radius to permit small space increments near the surface but larger time increments farther out in the solid medium.

A flow diagram of the Oracle code is given in Fig. 4. A time increment Δt was chosen to meet stability requirements for T_1 through T_5 and the

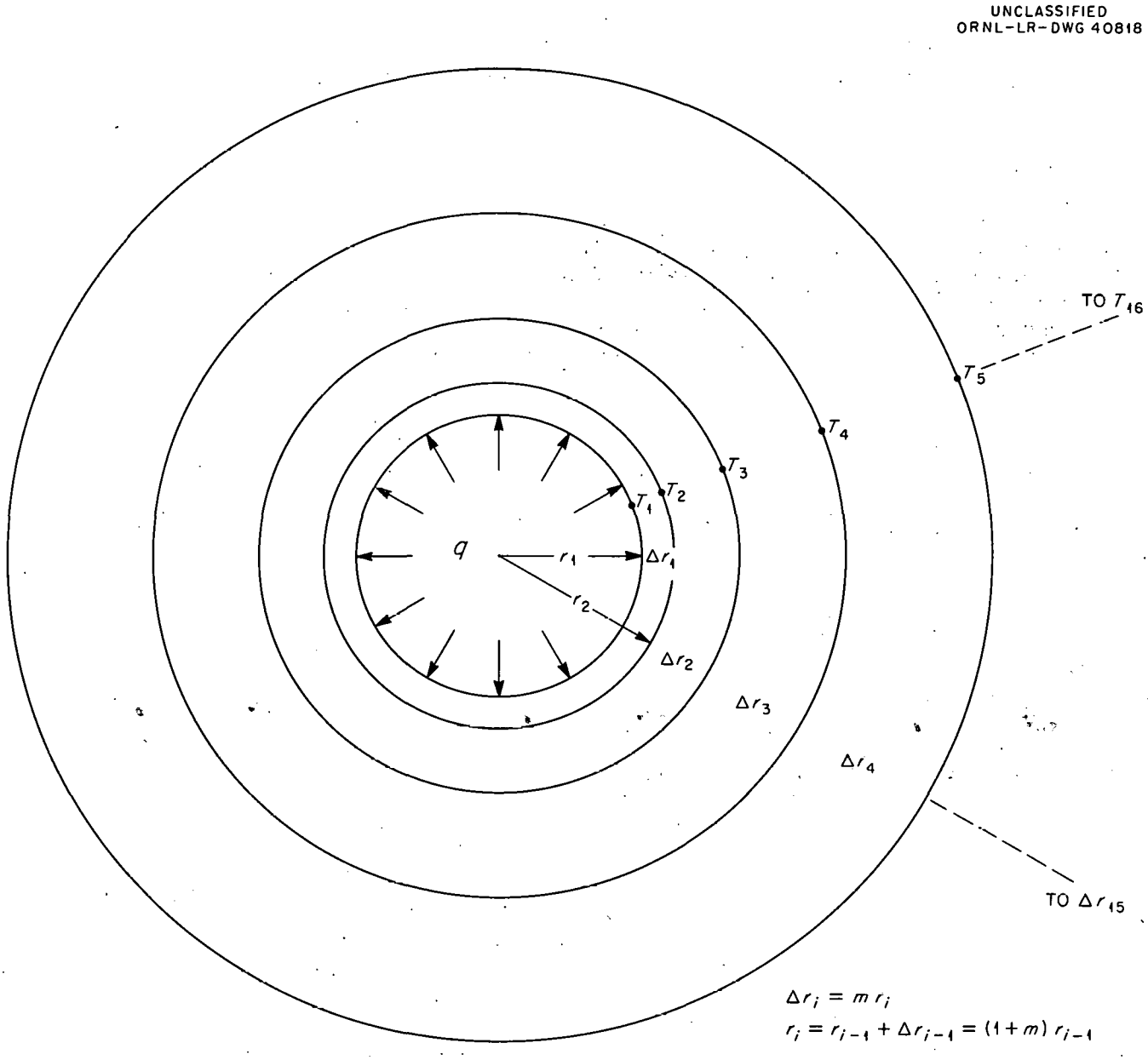

Fig. 3. Incremental Division of Infinite Solid Meduim for Derivation of Finite Difference Equations.

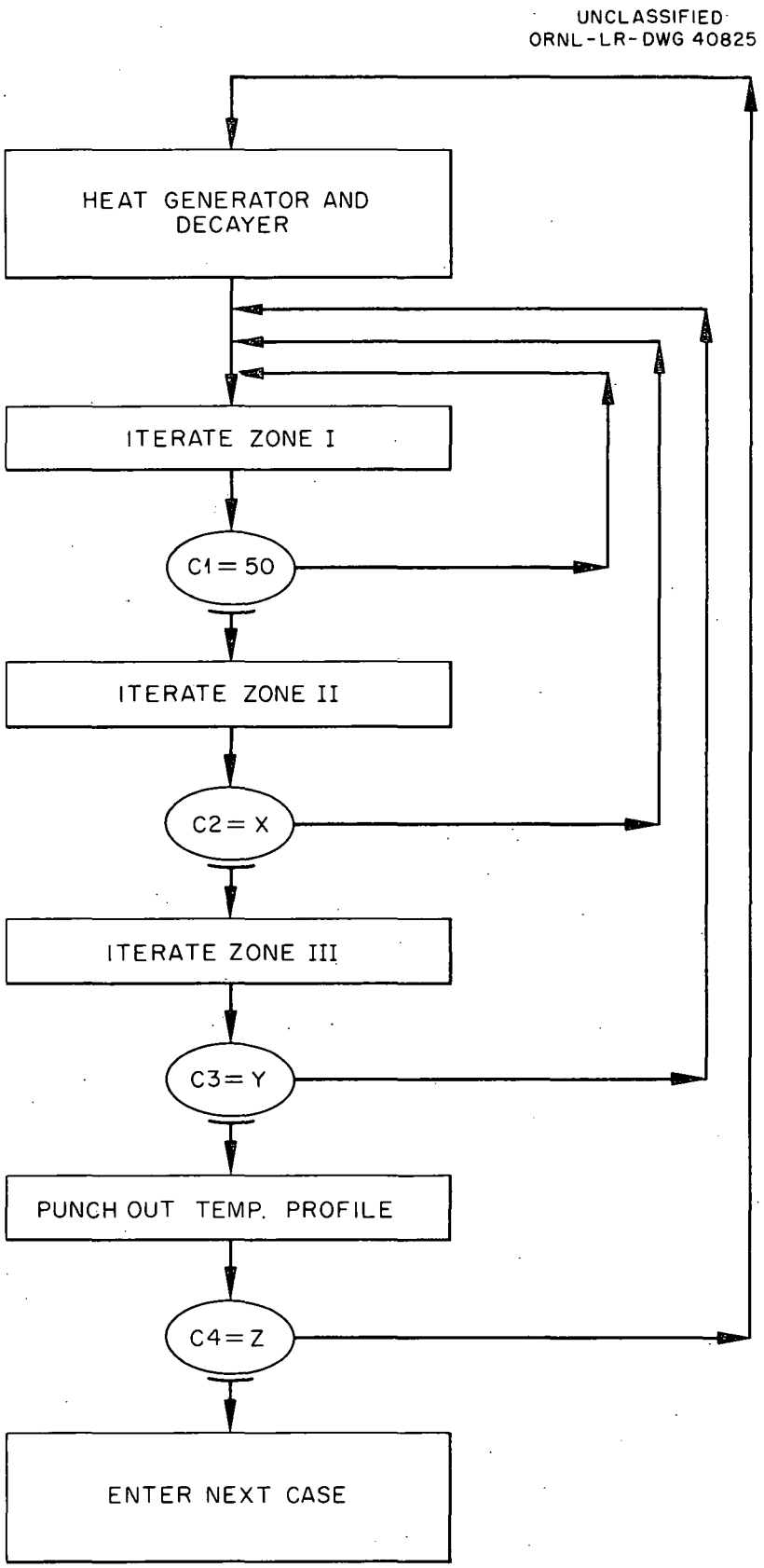

Fig. 4. Flow Diagram of Oracle Code.

proper values for the constants M_1 were incorporated in the code. Fifty iterations were carried out for zone I and then an iteration was done of zone 2, which had a time increment of 50 Δt. The process was repeated for X iterations of zone [redacted] followed by an iteration of zone III. The counter Y was set to cause the calculation of a new heat generation rate after sufficient time had elapsed for a decrease of about 5%. Counter Z stopped the calculation after a sufficient amount of storage time had elapsed to show the maximum temperature. A copy of the code is given in the appendix (Sec. 7.3).

3.2 Storage Model Assumptions

The temperature rise calculations were based on the following assumptions:

a. The temperature distribution in the cylinder at any time is the steady-state temperature distribution consistent with the instantaneous heat generation rate.

b. All thermal properties are independent of temperature.

c. The energy of fission product decay is dissipated uniformly within the radioactive solid cylinder.

d. No chemical reactions or changes of state occur.

e. The sensible heat of the radioactive solid is negligible compared with the heat generated up to the time that the maximum temperature is reached.

f. The temperature difference between the cylinder wall and the surrounding solid medium is determined by the instantaneous heat flux through two air films.

g. The surrounding medium is initially at uniform temperature.

As shown by the calculations in Sec. 2.2, cylinders of the sizes and with the properties of interest would closely approach steady state in 30 to 150 hr. Thus if at least a week or two of handling and transportation was required prior to ultimate storage, assumption a would be closely approximated at the time of storage and would continue to be good as the temperature distribution in the cylinder responded to the differentially changing cavity surface temperature.

The assumption that the thermal properties are independent of temperature does not lead to serious error in the calculation of cavity surface temperatures because the temperature rise in the storage medium is only moderate if the axial cylinder temperatures are limited to 1000°F and the conductivities are in the range 0.1 to 1.0 Btu/hr·ft°·F. In the radioactive solid cylinder, where the temperature changes are greater, the error is more serious; however, corrections cannot be made unless a particular material is chosen for which the effect of temperature on thermal conductivity is known.

Assumption c is well justified because most of the energy evolved by the Ce-144 chain and all by the Sr-90 chain is due to beta decay. Most of the energy evolved by the Cs-137 chain is due to the gamma decay of the Ba-137 daughter, but these photons are not very energetic (0.661 Mev). This assumption is on the conservative side, since greater distribution of the generated heat lowers the axial temperature.

With reference to assumption e, the volumetric heat capacities of calcined metal oxides and glasses are of the order of 10 to 30 Btu/ft^3.°F.[1,2] Thus, for an average temperature rise of 500°F, sensible heats of the order of 5000 to 15,000 Btu/ft^3 are produced. Over the range of heat generation rates of interest, these sensible heats are negligible compared with the total heat generated up to the time the maximum temperature is reached.

Two air films were assumed to determine the temperature difference between the cylinder and cavity surfaces since heat transfer across very tall enclosed air spaces is not well understood. The Grashof number, based on the 1-in. clearance, was greater than 10^4, showing that conduction would not be controlling.[16]

4.0 HEAT GENERATION RATES

Heat generation rates were calculated for Army Package Power Reactor (APPR-1) fuel reprocessed by the Darex Process.[17] For an average thermal flux of 2.7×10^{13} neutrons/cm^2·sec and an irradiation time of 1.9 years at 80% load factor,[18] fission product concentrations were calculated for decay times of one, three, and eight years.[19] Eight nuclides were found to be significant heat producers in one-year-decayed fuel and five nuclides in three- and eight-year-decayed fuel (Table 1). The solvent extraction flowsheet[17] specified 240 liters of raffinate solution from the first extraction column per kilogram of uranium fed. All fission products were assumed to have remained in this raffinate, and a concentration factor of 8 was assumed for the conversion of the raffinate to solid form. These calculations resulted in heat generation rates of approximately 700, 210, and 70 Btu/hr per cubic feet of solid for one-, three-, and eight-year-decayed materials. Details of these calculations are given in the appendix (Sec. 7.1). A graph of heat generation rate as a function of time, normalized to one-year decayed material, is given in Fig. 14 (appendix).

Heat generation rates for the APPR-1 fuel were regarded merely as representative values, and temperature rise calculations were carried out with heat generation rates up to 2000 Btu/hr per cubic foot of solid. While the fission product distribution from slightly enriched power reactor fuels with higher burnups are somewhat different from those of the fully enriched APPR-1, they are dominated by Ce-144 after one year of decay time and by Sr-90 and Cs-137 after eight years and do not cause a significant difference in the temperature rise values.

Table 1. Fraction of Heat Generation Rate for Various Nuclides[a] from APRR-1 Fuel

Nuclide	Decayed 1 year	Decayed 3 years	Decayed 8 years
Sr-89	0.007	--	--
Y-91	0.013	--	--
Zr-95—Nb-95	0.057	--	--
Ce-144	0.721	0.456	0.015
Ru-106	0.051	0.047	0.004
Pm-147	0.017	0.036	0.024
Sr-90	0.081	0.278	0.579
Cs-137	0.053	0.183	0.378
	1.000	1.000	1.000

[a] The decay energy from its daughter was attributed to the nuclide listed. Transient equilibrium was assumed in all cases.

5.0 RESULTS

5.1 Cavity Surface Temperature as a Function of Time

By means of the Oracle code cavity surface temperatures were calculated for cavities with radii ranging from 5 to 30 in. The time for the maximum temperature of the cavity surface to be reached depended primarily on the decay rate of the heat flux and was only slightly affected by the physical properties of the solid medium. For heat fluxes decaying like one-, three-, and eight-year-decayed reactor wastes, temperature maxima were reached in about three months, six months, and six years of storage time.

Temperature-time curves for the surface of a cavity in an infinite medium of "average soil" showing the effect of decay time are given in Fig. 5. Temperature-time curves for the surface of a cavity in an infinite salt medium showing the effects of cavity radius and magnitude of heat flux are given in Figs. 6a - c and 7. By the methods of Sec. 2.2, assuming constant heat flux with time, temperature-time curves were drawn for comparison. The constant heat flux calculations served as a check on the convergence of the finite difference equations, showing good agreement in all cases.

The physical properties of interest of "average soil," "average rock," and salt are given in Table 2.

5.2 Temperature Profiles in the Infinite Medium

A few examples of temperature profiles in the infinite medium are given in Fig. 8a - c, including in each case the profile at the time of maximum surface temperature. The calculation grid extended to a radial distance of 297 ft for the 10-in. radius, to 447 ft for the 15-in. radius and to 894 ft for the 30-in. radius, at which points an isothermal boundary was assumed. The validity of this assumption is confirmed by the fact that the thermal gradient had not progressed to these distances by the end of the calculations for any case examined.

5.3 Temperature Rise at the Radioactive Cylinder Axis as a Function of Time

The temperature rise in the radioactive cylinder above the initial ground temperature was computed by adding the temperature drop through the radioactive cylinder, the temperature drops across the convection film at the cylinder and cavity surfaces, and the temperature rise of the cavity surface above the initial ground temperature. The temperature drop from the axis to the surface of the radioactive cylinder was found from eq. 17 to be

$$T_{r=0} - T_{r=R} = \frac{QR^2}{4k} \qquad (25)$$

Temperature drops across the convection films at the cylinder and cavity surfaces were calculated by

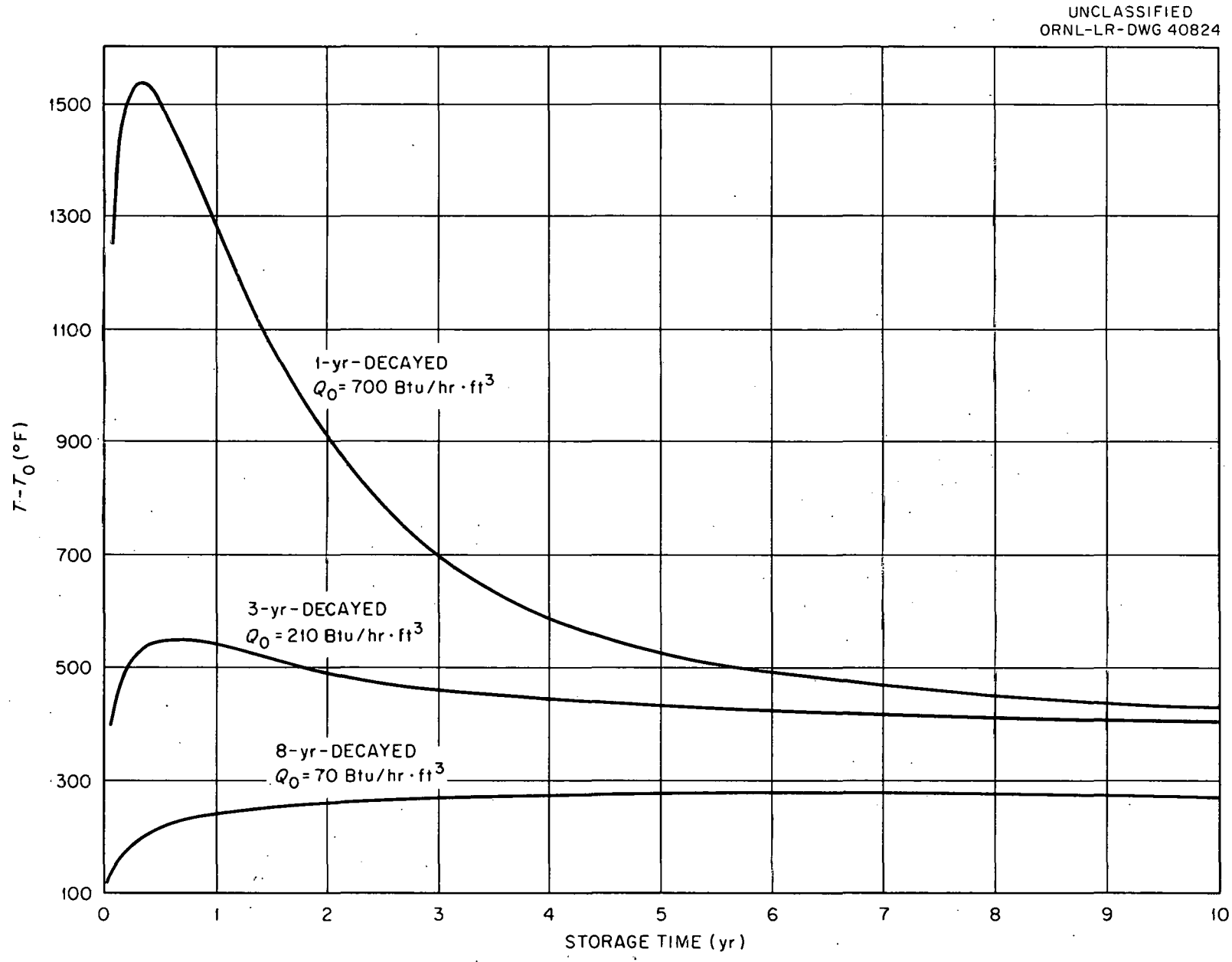

Fig. 5. Temperature Rise at the Cavity Surface as a Function of Storage Time, Showing the Effect of Decay Time. Cavity Radius = 15 in. Soil Medium.

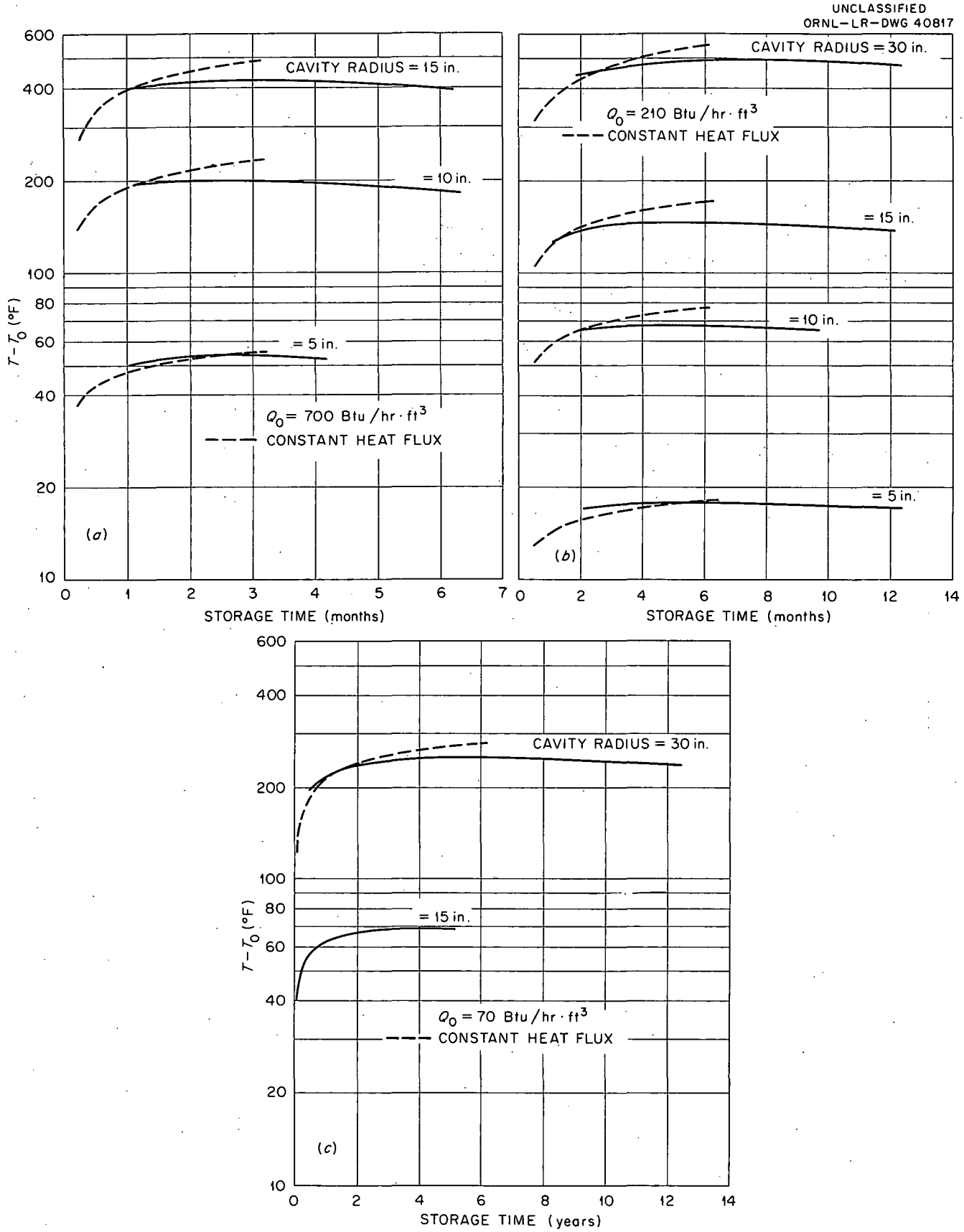

Fig. 6. Temperature Rise at the Cavity Surface as a Function of Storage Time and Cavity Radius for Material Decayed (*a*) One Year, (*b*) Three Years, and (*c*) Eight Years Prior to Storage. Salt Medium.

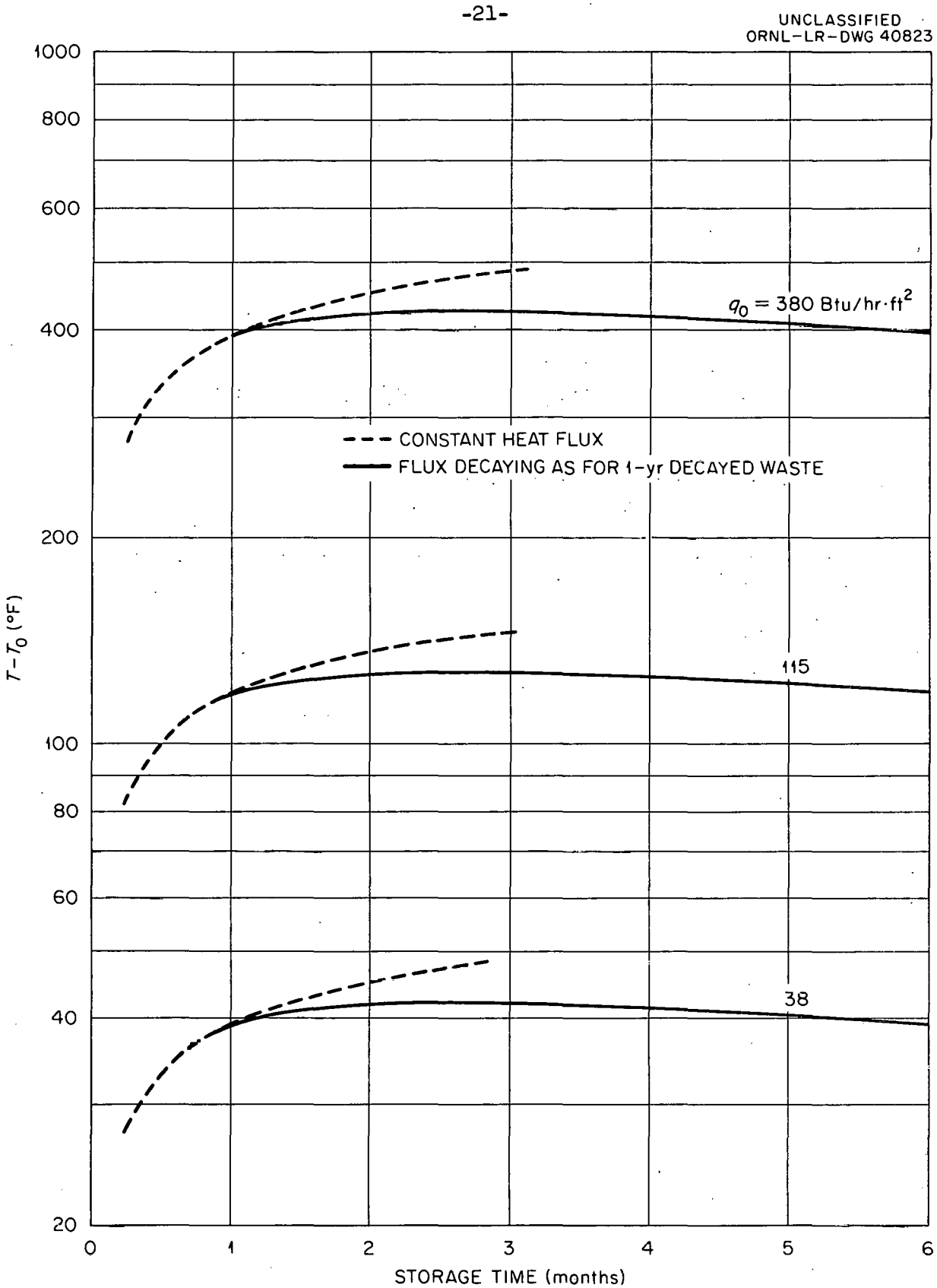

Fig. 7. Temperature Rise at Cavity Surface as a Function of Storage Time and Heat Flux at Constant Cavity Radius of 15 in. Salt Medium.

Table 2. Physical Properties of Various Media

Medium	Thermal Conductivity, Btu/hr·ft·°F	Thermal Diffusivity, ft^2/hr
Average soil[20]	0.56	0.0178
Average rock[20]	1.0	0.0457
Salt[21,22]	2.80 (100°C)	0.101

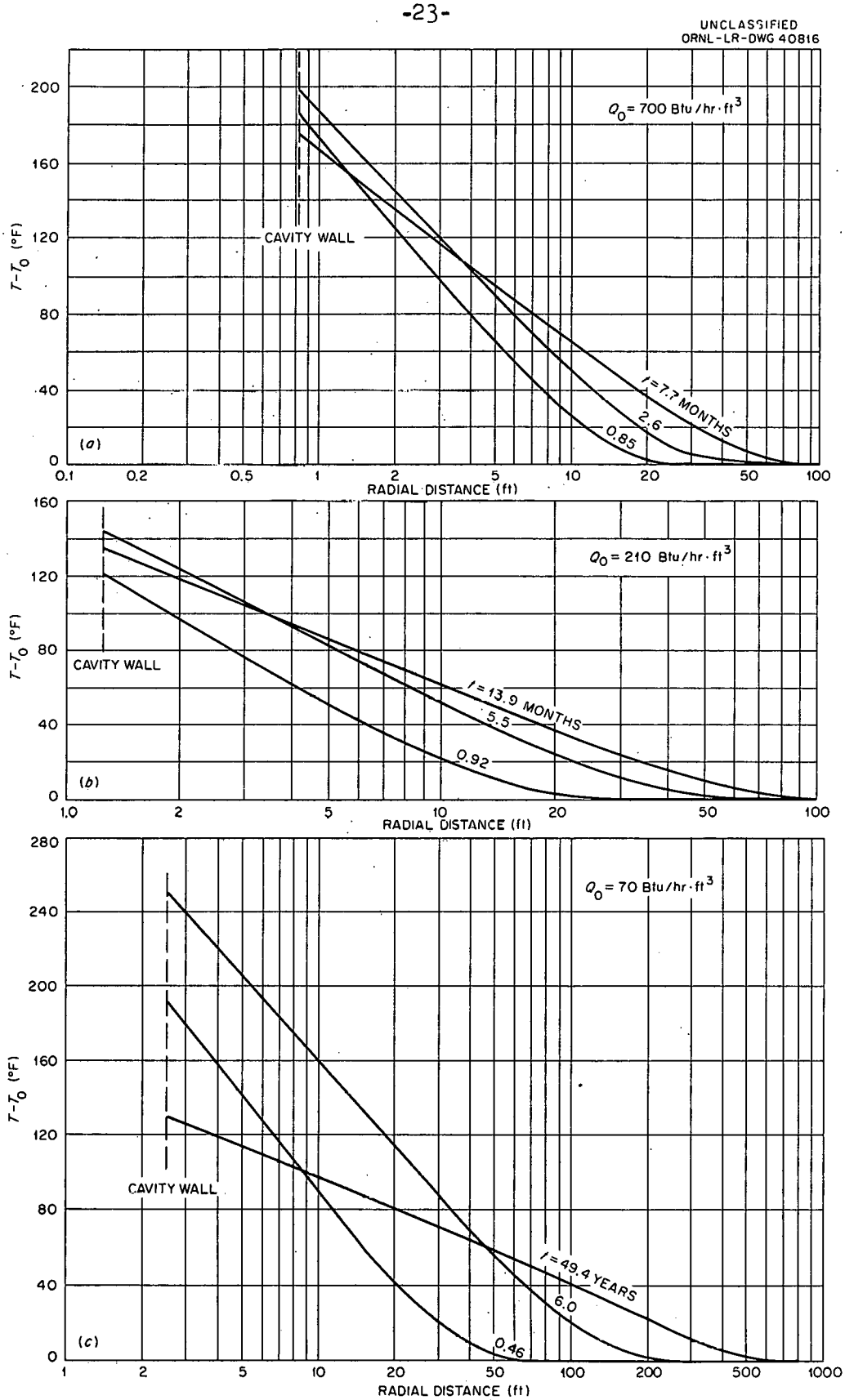

Fig. 8. Temperature Profiles in an Infinite Salt Medium, as a Function of Radial Distance and Storage Time of Radioactive Waste Decayed (*a*) One Year (Cavity Radius 10 in.) (*b*) Three Years (Cavity Radius 15 in.) (*c*) Eight Years (Cavity Radius 30 in.) Prior to Storage.

$$T_{r=R} - T_A = \frac{QR}{2h} \quad \text{and} \quad T_A - T_{r=R_2} = \frac{QR^2}{2hR_2} \tag{26}$$

The heat generation rate Q decreased with time according to Fig. 14 (appendix), while the temperature rise of the cavity surface was obtained from Figs. 5-7. Because of the more direct dependence of the temperature drops through the radioactive cylinders and across the air gap on the decreasing heat generation rate, their contribution to the temperature rise caused the maximum center-line temperature to occur considerably before the maximum at the cavity surface.

The time required for the temperature at the radioactive cylinder axis to reach a maximum decreased as the thermal conductivity of the radioactive cylinder decreased, again because of the increased fraction of the total temperature rise due to the cylinder itself. With a thermal conductivity of 0.1 Btu/hr·ft·°F, the maximum temperatures for one-, three-, and eight-year-decayed materials were reached in about one week, two weeks, and seven months of storage time. Thus the temperature at the cylinder axis reaches its maximum before the heat generation rate has decreased significantly, and the methods of Sec. 2.2, which assume constant heat flux, may be used here. The temperature rise at the radioactive cylinder axis as a function of storage time for a few sample cases is given in Fig. 9a - c.

5.4 Effects of Thermal Conductivity of Radioactive Cylinder and Convection Coefficient on Maximum Temperature Rise

The maximum temperature rise increased sharply as the thermal conductivity of the radioactive cylinder was decreased below 0.1 Btu/hr·ft·°F. The influence of the convection coefficient became less important as the radius increased, since the temperature drop across the convection film is inversely proportional to radius while the temperature drop through the radioactive cylinder is proportional to r^2. These effects are illustrated in Fig. 10a - d.

5.5 Effects of Decay and Dilution Prior to Storage

The specific heat generation rate of a radioactive material can be decreased prior to ultimate storage by (1) allowing the material to decay in a temporary storage system, or (2) diluting with a nonradioactive material. Thus, by manipulating these two alternatives, wastes with different fission product spectra but the same specific heat generation rates can be produced. For two materials with the same specific heat generation rates but different fission product spectra, the one with the slower decay rate would be expected to result in a higher maximum temperature rise upon storage. Over the range of conditions studied, the effect was found to be small. The difference in maximum temperature rise between one- and three-year-decayed materials was about 2% and between one- and eight-year-decayed materials about 7% (Fig. 11).

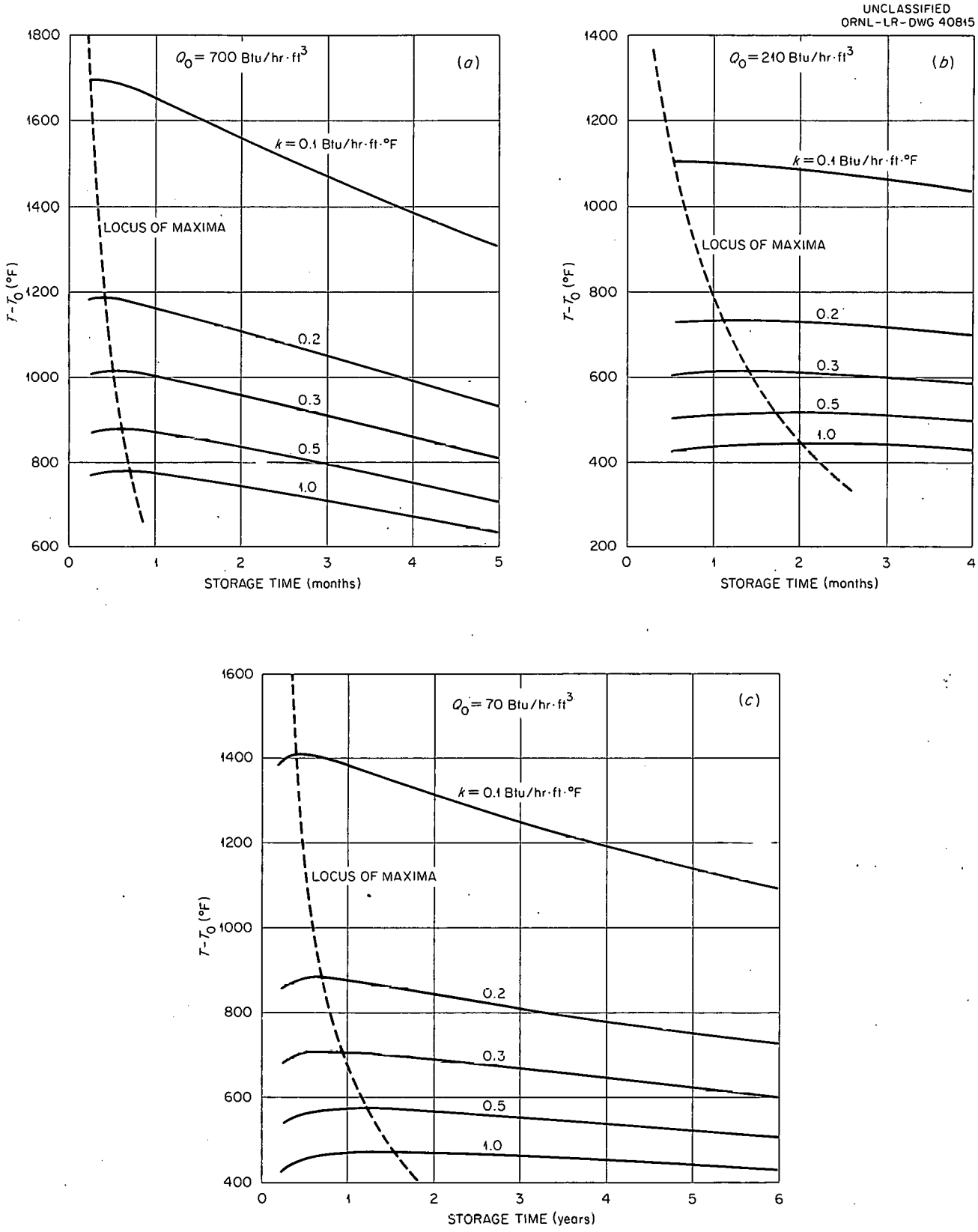

Fig. 9. Temperature Rise at the Axis of a Cylinder of Radioactive Waste as a Function of Storage Time and Thermal Conductivity for Material Decayed (*a*) One year (Cavity Radius 10 in.) (*b*) Three years (Cavity Radius 15 in.) and (*c*) Eight years (Cavity Radius 30 in.) Prior to Storage. Salt Medium, $h = 1.0$ Btu/hr·ft^2·°F.

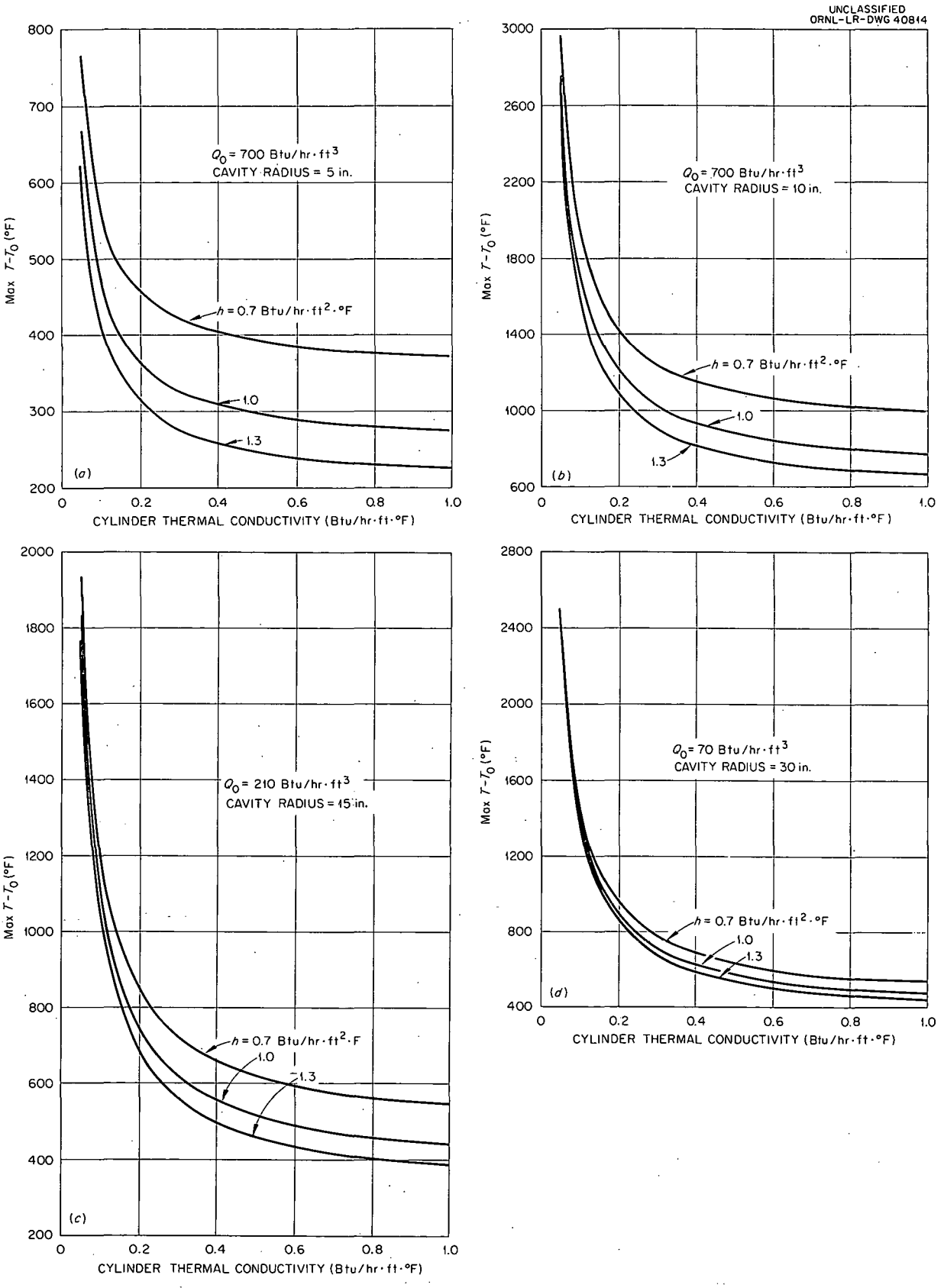

Fig. 10. Maximum Temperature Rise in a Cylinder of Radioactive Waste as a Function of Thermal Conductivity of the Cylinder and the Convection Coefficient in the Air Space of Material Decayed (*a*,*b*) One Year, (*c*) Three Years, and (*d*) Eight Years Prior to Storage. Salt Medium.

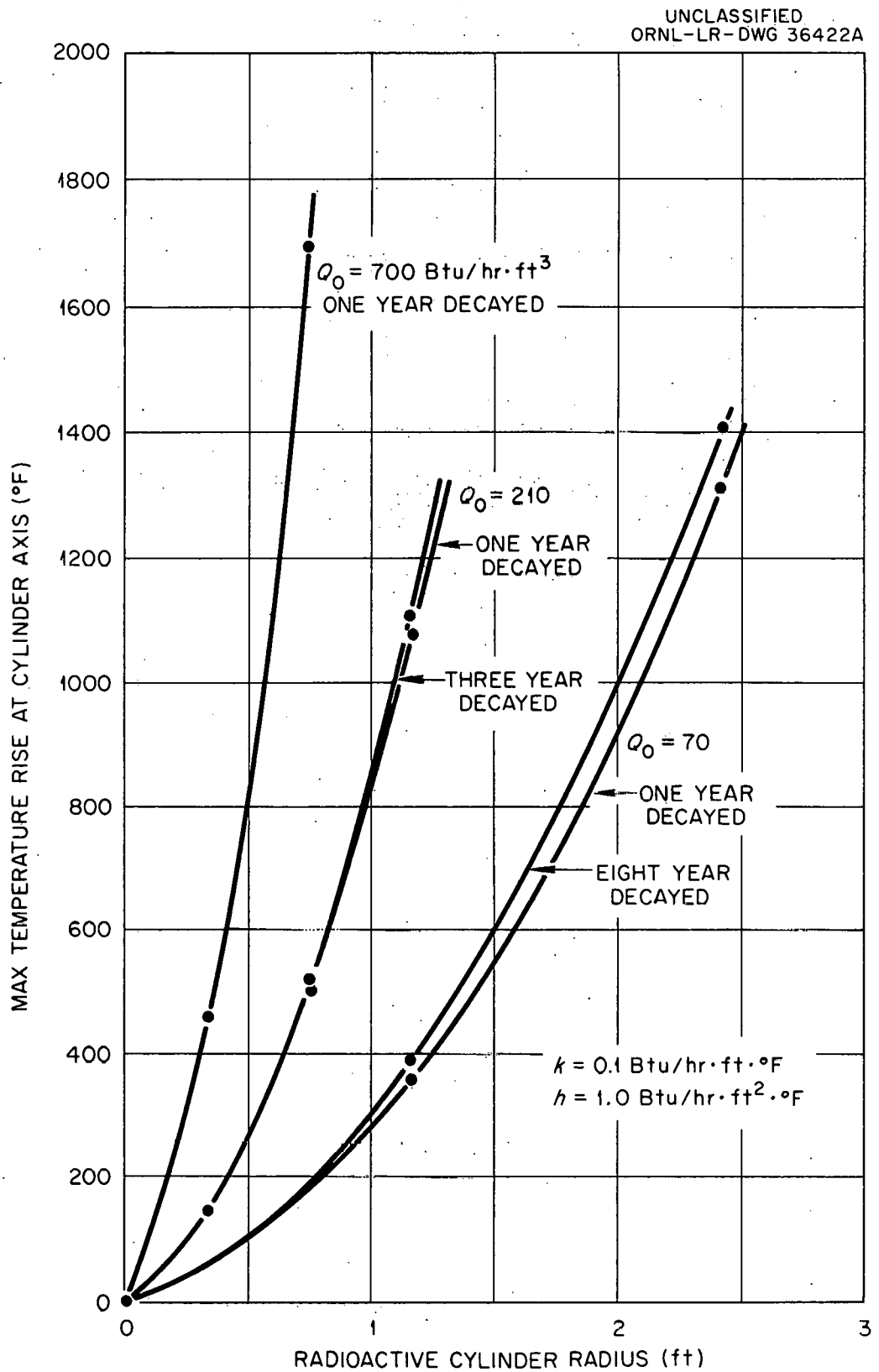

Fig. 11. Temperature Rise at the Axis of a Cylinder of Radioactive Waste as a Function of Radius and Heat Generation Rate. Salt Medium.

5.6 Comparison of Storage in Soil, Rock, and Salt Media

The thermal conductivities and thermal diffusivities of "average soil," "average rock," and salt are given in Table 2. The temperature rise at the axis of the radioactive cylinder was calculated for storage in these media assuming thermal conductivities of 0.1 and 0.3 Btu/hr·ft·°F for the cylinder (Fig. 12a,b). For a given initial heat generation rate and cylinder radius, the maximum temperature rise for storage in "average soil" was 25 to 50% higher than for storage in salt and 10 to 20% higher than for storage in "average rock." As the thermal conductivity of the cylinder increases, the choice of storage medium becomes more important because a smaller fraction of the total allowable temperature rise occurs in the radioactive cylinder.

5.7 Storage with Constant Air Temperature

While the assumed storage model has several advantages from an operational viewpoint, it is probably the most conservative storage method with regard to minimizing temperature rise. A method that would give a lower maximum temperature rise would be to cool the radioactive cylinders with a fluid from a constant-temperature source circulating by natural convection. Assuming that water is not a permissible fluid for ultimate disposal of radioactive wastes because of corrosion or leaching considerations, air might be used as the coolant fluid.

The temperature difference at steady state between the axis and the surface of a cylinder with constant uniform heat generation is given by eq. 25. The temperature difference across the air film at the surface of the cylinder is given by eq. 26. Assuming that the cylinder is in a vertical position and cooled by natural convection in air, the convection coefficient is given by eq. 18. Combining eqs. 26 and 18 yields

$$T_{r=R} - T_A = 1.88RQ^{0.80} \tag{27}$$

Thus the axial temperature rise of the radioactive cylinder above ambient is given by

$$T_{r=0} - T_A = \frac{QR^2}{4k} + 1.88RQ^{0.80} \tag{28}$$

Equation 28 was used to calculate a few cases of interest (Fig. 13). Infinite-medium cases with radioactive solids of thermal conductivity of 0.1 Btu/hr·ft·°F are replotted here for comparison. For storage in a constant-temperature air sink with natural convection cooling rather than in an infinite salt medium, the permissible heat generation rate is increased about 50%.

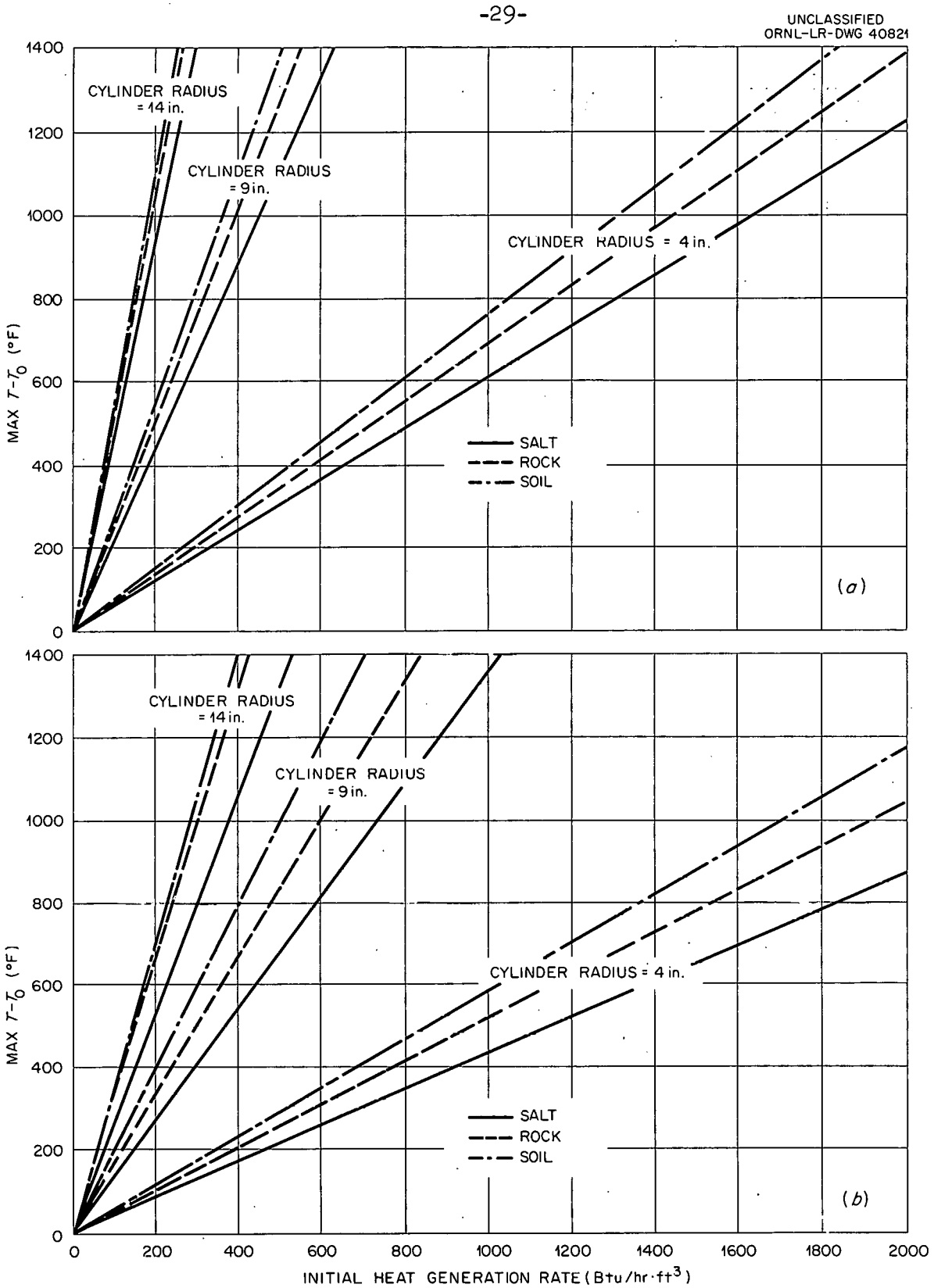

Fig. 12. Maximum Temperature Rise at the Axis of a Cylinder of Radioactive Waste Decayed One Year Prior to Storage as a Function of Heat Generation Rate and Cylinder Radius for Various Storage Media. $h = 1.0$ Btu/hr·ft^2·°F, (*a*) (k) = 0.1 Btu/hr·ft·°F, (*b*) k = 0.3 Btu/hr·ft·°F.

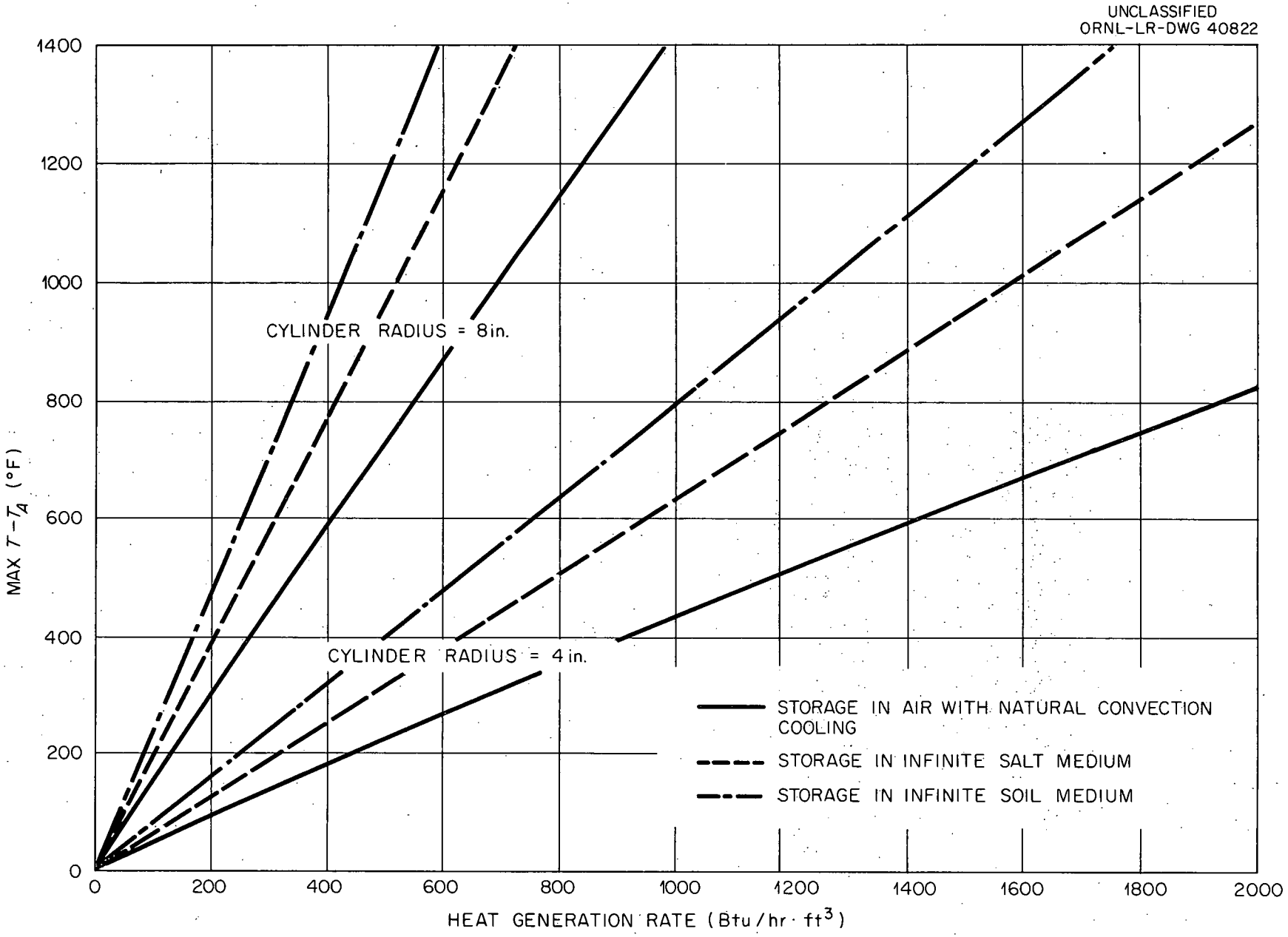

Fig. 13. Maximum Axial Temperature Rise of Stored Radioactive Cylinders as A Function of Heat Generation Rate. Thermal Conductivity of Radioactive Solid = 0.1 Btu/hr·ft·°F.

6.0 REFERENCES

1. E. S. Grimmett, "Calcination of Aluminum-Type Reactor Fuel Wastes in a Fluidized Bed," IDO-14416 (Aug. 1, 1957).

2. C. W. Hancher, "Reduction of Radioactive Waste to Solids for Ultimate Storage," ORNL-CF-59-1-77 (Jan. 28, 1959).

3. L. P. Bupp, Monthly Report, Chemical Research and Development Operation, p. C-5, HW-59099C (January 1959).

4. A. A. Jonke et al., Chemical Engineering Summary Reports, ANL-5422 (May 3, 1955), 5466 (July 27, 1955), 5529 (Feb. 10, 1956).

5. J. M. White and G. Lahie, "Ultimate Fission Product Disposal. Disposal of Curie Quantities of Fission Products in Siliceous Materials," CRCE-591 (March 1955).

6. W. S. Ginell, J. J. Martin, and L. P. Hatch, "Ultimate Disposal of Radioactive Wastes," Nucleonics, 12, No. 12, pp. 14-18 (1954).

7. C. B. Amphlett and D. T. Warren, "Fixation of Activity in Solid Form by Adsorption on Soils," AERE-C/R 2202 (April 1957).

8. L. C. Watson et al., "Methods of Storage of Solids Containing Fission Products," CRCE-736 (June 1958).

9. J. K. Perring, "The Cooling of Underground Fission Wastes," AERE-C/R-1294 (Nov. 9, 1953).

10. "Symposium on the Reprocessing of Irradiated Fuels," May 20-25, 1957, TID-7534, Book 1, p. 444.

11. H. S. Carslaw and J. C. Jaeger, "Conduction of Heat in Solids," 1st ed., p. 176, Oxford Press, London, 1947.

12. W. H. McAdams, "Heat Transmission," 2nd ed., pp. 241 and 246, McGraw-Hill, New York, 1942.

13. N. A. Lange, Editor, "Handbook of Chemistry," 9th ed., pp. 1557 and 1541, Handbook Publishers, Sandusky, Ohio, 1956.

14. Carslaw and Jaeger, op. cit., p. 283.

15. H. S. Mickley, T. K. Sherwood, and C. S. Reed, "Applied Mathematics in Chemical Engineering," p. 357, McGraw-Hill, New York, 1957.

16. McAdams, op. cit., 3rd ed., p. 181, 1954.

17. J. R. Flanary and J. H. Goode, "Recovery of Enriched Uranium from Uranium Dioxide-Stainless Steel Fuel Elements by Solvent Extraction," ORNL-CF-58-4-2 (April 3, 1958).

18. J. W. Ullmann, ORNL, personal communication, Nov. 8, 1957.

19. J. O. Blomeke and M. F. Todd, "Uranium-235 Fission-Product Production as a Function of Thermal Neutron Flux, Irradiation Time, and Decay Time," ORNL-2127 (Aug. 19, 1957).

20. Carslaw and Jaeger, op. cit., Appendix VI.

21. "Handbook of Chemistry," op. cit., pp. 307 and 1542.

22. J. H. Perry, Editor, "Chemical Engineers Handbook," 3rd ed., p. 223, McGraw-Hill, New York, 1950.

7.0 APPENDIX

7.1 Calculation of Heat Generation Rates

For a thermal flux of 2.7×10^{13} neutrons/cm^2·sec and an irradiation time of 6.0×10^7 sec, the fission product growth calculations are summarized in Table 3.

Assuming 29 gal of liquid waste produced per pound of U-235 reprocessed, as in the Darex flowsheet,[17]

$$\left(\frac{1 \text{ lb U-235}}{29 \text{ gal liq waste}}\right)\left(\frac{454 \text{ g}}{\text{lb}}\right)\left(\frac{\text{g-mole}}{235 \text{ g}}\right) = 0.0667 \text{ g-mole U-235 per gal liq waste}$$

Assuming a concentration factor of 8 from evaporation and calcination,

$$\left(\frac{8 \text{ gal liq waste}}{\text{gal solid waste}}\right)\left(0.0667 \frac{\text{g-mole U-235}}{\text{gal liq waste}}\right) = 0.534 \text{ g mole U-235 per gal solid waste}$$

Therefore

$$\left(\frac{0.534 \text{ g-mole U-235}}{\text{gal solid waste}}\right)\left(\frac{Nt}{N_{25}^{\circ}} \frac{\text{g-mole f.p.}}{\text{g-mole U-235}}\right)\left(6.02 \times 10^{23} \frac{\text{atoms}}{\text{g-mole}}\right)\left(\lambda \frac{\text{dis}}{\text{hr}}\right) \times$$

$$\times \left(E \frac{\text{Mev}}{\text{dis}}\right)\left(1.52 \times 10^{-16} \frac{\text{Btu}}{\text{Mev}}\right) = 4.89 \times 10^7 \left(\frac{Nt}{N_{25}^{\circ}}\right)(\lambda)(E) \text{ Btu/hr·gal solid}$$

The radiation energies and specific heat generation rates for the important fission products are given in Table 4. Figure 14 was obtained by the use of Fig. T-18a, p. 355, of reference 19.

Table 3. Calculation of Fission Product Concentrations in APPR Fuel

Nuclide	Saturation Value (N_s/N°_{25})	Fraction of Saturation (N_τ/N_s)	Fraction of Shutdown (N_t/N_τ)			N_t/N°_{25}, moles/mole		
			1 year	3 years	8 years	1 year	3 years	8 years
Sr-89	5.0×10^{-3}	1.0	1.0×10^{-2}	--	--	5.0×10^{-5}	--	--
Y-91	6.7×10^{-3}	1.0	1.5×10^{-2}	--	--	1.0×10^{-4}	--	--
Zr-95—Nb-95	8.0×10^{-3}	1.0	1.8×10^{-2}	--	--	1.44×10^{-4}	--	--
Ce-144	3.45×10^{-2}	0.78	0.43	7.4×10^{-2}	1.0×10^{-3}	1.16×10^{-2}	1.99×10^{-3}	2.69×10^{-5}
Ru-106	2.7×10^{-3}	0.71	0.49	0.122	4.0×10^{-3}	9.39×10^{-4}	2.34×10^{-4}	7.66×10^{-6}
Pm-147	4.0×10^{-2}	0.43	0.83	0.48	0.13	1.43×10^{-2}	8.26×10^{-3}	2.23×10^{-3}
Sr-90	1.2	4.8×10^{-2}	1.0	0.94	0.80	5.80×10^{-2}	5.41×10^{-2}	4.50×10^{-2}
Cs-137	1.0	5.2×10^{-2}	1.0	0.94	0.80	5.20×10^{-2}	4.89×10^{-2}	4.05×10^{-2}

Table 4. Specific Heat Generation Rates for Important Fission Products

Nuclide	Avg. (E_b) + Total (E_g), Mev			λ, hr^{-1}	Q_o, Btu/hr·gal solid		
	Parent	Daughter	Total		1 year	3 years	8 years
Sr-89	0.487	Stable	0.487	5.33×10^{-4}	0.63	--	--
Y-91	0.512	Stable	0.512	4.97×10^{-4}	1.24	--	--
Zr-95--Nb-95	0.860	0.798	1.658	4.57×10^{-4}	5.33	--	--
Ce-144	0.130	1.05	1.18	9.93×10^{-5}	66.50	11.40	0.15
Ru-106	0.013	1.30	1.31	7.92×10^{-5}	4.76	1.19	0.04
Pm-147	0.074	Stable	0.074	3.04×10^{-5}	1.57	0.91	0.24
Sr-90	0.20	0.73	0.93	2.83×10^{-6}	7.47	6.97	5.80
Cs-137	0.19	0.661	0.798	2.40×10^{-6}	4.87	4.58	3.79
					92.37	25.05	10.02

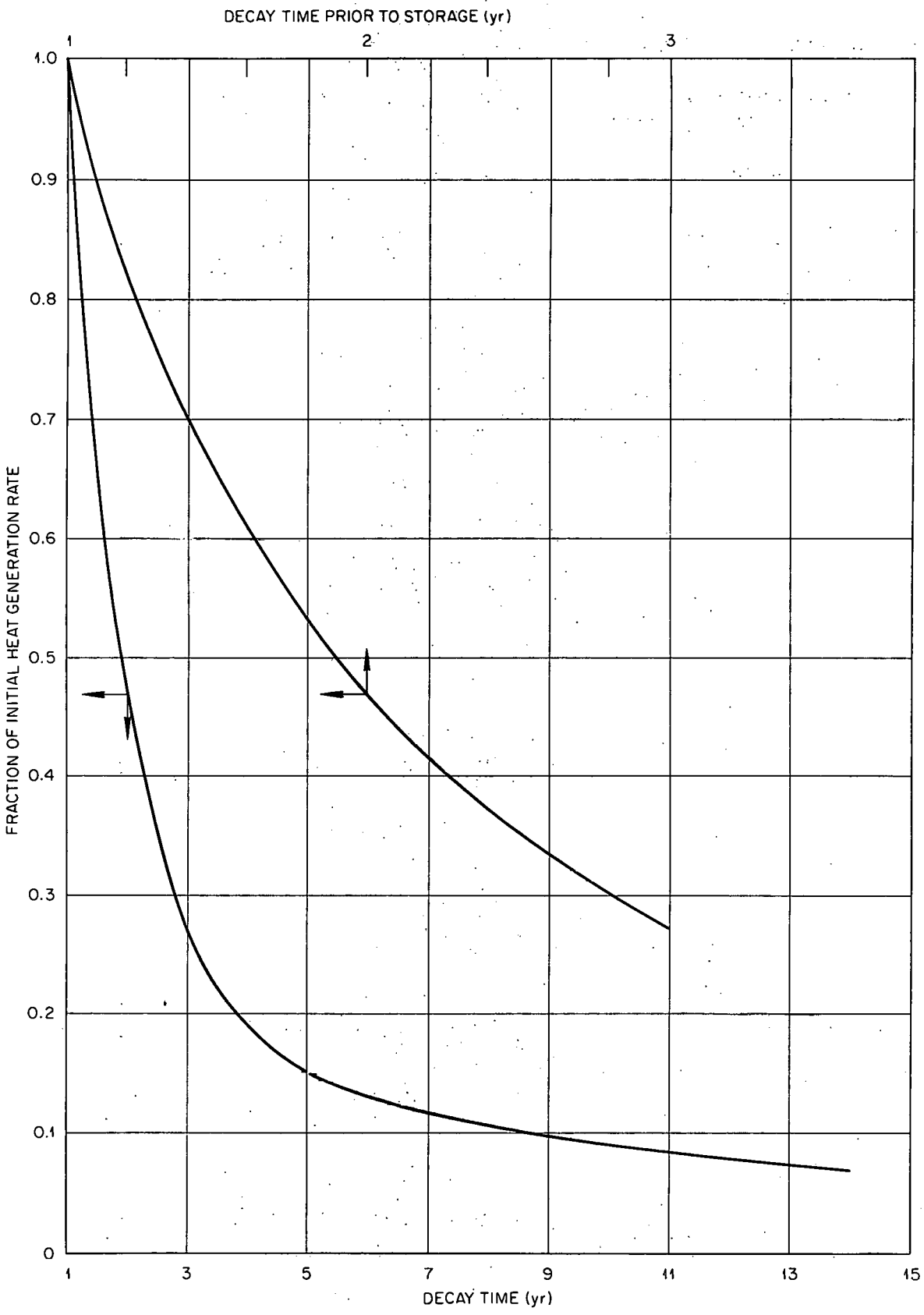

Fig. 14. Normalized Heat Generation Rate as a Function of Decay Time. Thermal Neutron Flux = 2.7×10^{13} neutrons/cm^2 · sec, Irradiation Time = 6.0×10^7 sec.

7.2 Derivation of Finite Difference Equations

The expression for T_1 is obtained by a heat balance between r_1 and the log mean of r_1 and r_2; basis 1 ft of height.

Input: q Btu/hr·ft^2 = $q\ A_1\ \Delta t$ Btu = $q \times 2\pi r_1\ \Delta t$

Output: $\dfrac{kA_{1,2}(T_{1,t} - T_{2,t})\ \Delta t}{\Delta r_1}$ where $A_{1,2} = \dfrac{A_2 - A_1}{\ln (A_2/A_1)} = \dfrac{2\pi(r_2 - r_1)}{\ln (r_2/r_1)}$

Let $\Delta r_i = mr_i$

$$r_i = r_{i-1} + \Delta r_{i-1} = (1 + m)r_{i-1}$$

then $A_{1,2} = \dfrac{2\pi[(1 + m)r_1 - r_1]}{\ln [(1 + m)r_1/r_1} = \dfrac{2\pi m r_1}{\ln (1 + m)}$

Accumulation: $\pi(r_{1,2}^2 - r_1^2)\rho c\ (T_{1,t + \Delta t} - T_{1,t})$

$$\pi\left[\left(\frac{mr_1}{\ln (1 + m)}\right)^2 - r_1^2\right]\rho c\ (T_{1,t + \Delta t} - T_{1,t})$$

Input - Output = accumulation

$$\frac{r_1 q \ln (1 + m)}{k} - (T_{1,t} - T_{2,t}) = r_1^2\left[\frac{m^2}{\ln (1 + m)} - \ln (1 + m)\right]\frac{\rho c}{2k\ \Delta t}(T_{1,t + \Delta t} - T_{1,t})$$

Let $M_1 = \dfrac{\rho c r_1^2}{2k\ \Delta t}\left[\dfrac{m^2}{\ln (1 + m)} - \ln (1 + m)\right]$

$$T_{1,t + \Delta t} = \frac{qr_1}{kM_1}(\ln 1 + m) + \frac{(M_1 - 1)\ T_{1,t} + T_{2,t}}{M_1}$$

The expression for T_i is obtained by a heat balance between $r_{i-1,i}$ and $r_{i,i+1}$.

Input: $$\frac{kA_{i-1,i}(T_{i-1,t} - T_{i,t})\ \Delta t}{\Delta r_{i-1}} = \frac{2\pi k(T_{i-1,t} - T_{i,t})\ \Delta t}{\ln (1 + m)}$$

Output: $$\frac{kA_{1,i+1}(T_{i,t} - T_{i+1,t})\ \Delta t}{\Delta r_i} = \frac{2\pi k(T_{i,t} - T_{i+1,t})\ \Delta t}{\ln (1 + m)}$$

Accumulation: $\pi(r_{i+1,i}^2 - r_{i,i-1}^2)\ \rho c(T_{i,t + \Delta t} - T_{i,t})$

$$\pi\left[\frac{m}{\ln(1+m)}\right]^2 (r_i^2 - r_{i-1}^2)\rho c(T_{i,t+\Delta t} - T_{i,t})$$

Input-output = accumulation

$$T_{i-1,t} - 2T_{i,t} + T_{i+1,t} = \frac{\rho c m^2(m^2+2m)r_{i-1}^2}{2k\,\Delta t \ln(1+m)} (T_{i,t+\Delta t} - T_{i,t})$$

Let $$M_i = \left(\frac{\rho c}{k}\right)\left[\frac{m^3(m+2)}{\ln(1+m)}\right]\frac{r_i^2 - 1}{2\,\Delta t}$$

$$T_{i,t+\Delta t} = \frac{T_{i-1,t} + (M_i - 2)\,T_{i,t} + T_{i+1,t}}{M_i}$$

7.3 Oracle Code

The code is loaded into the electrostatic memory from paper tape starting in cell 000. All constants must be loaded as hexadecimal numbers. Table 5 gives the location of the pertinent constants. Transfer to 000 to start code.

Since this is a fixed point code, some constants are multiplied by a scale factor of 2^{-16} prior to conversion to the hexadecimal system. A starred number is written assuming the binary point to the right of the register (e.g. 1* = 00 000 00 001). A diagram of the code showing the subroutine organization is given in Fig. 15.

Table 5. Oracle Code Constants

Location	Kind of Number	Constant
0EF	Starred	Sets loop counter for item 100
0F0	Fraction	$\frac{r_1 \ln(1+m)}{kM_1}$
0F1	Fraction	$M_1 - 1$
0F2 through 100	Scaled	M_1 through M_{15}
101 through 10E	Scaled	$(M_2 - 2)$ through $(M_{15} - 2)$
10F through 116	Scaled	Initial heat generation rates (Btu/hr.ft^2) for the eight nuclides of one-year decayed material
117 through 11E	Fraction	$1 - \lambda\Delta t$ for eight nuclides
11F through 128	Scaled	Initial heat generation rates for the five nuclides of three- and eight-year decayed material
133	Starred	Sets loop counter for item 200
134	Starred	Sets loop counter for item 300
135	Starred	Sets loop counter for item 010

UNCLASSIFIED
ORNL-LR-DWG 40819

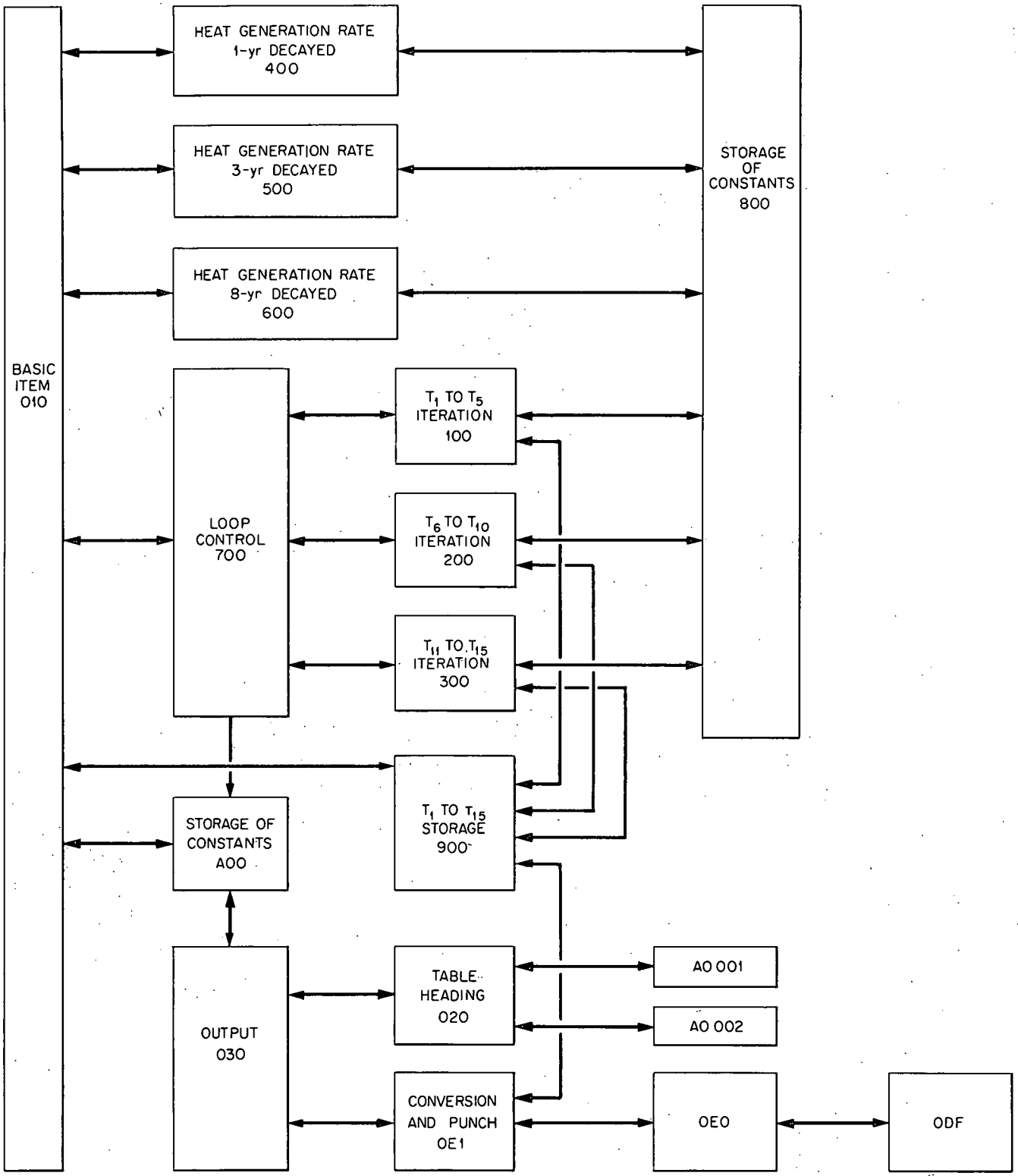

Fig. 15. Diagram of Oracle code.

Oracle Code with Constants Set for a Cavity Radius of 10 In.

Directory

```
0000000010 0000100400 0000200500 0000300600
0000400700 0000500100 0000600200 0000700300
0000800030 0000900020 0000aa0001 0000ba0002
0000c00800 0000d00900 0000e00a00 ffffffffff
001ab00000 00623001ab ffffffffff 0019700e00
0019800e01 0019900e10 0019a00e2b 0019b00e2c
0019c00e2d 0019d00e78 0019e00e80 0019f00e8a
001a000ea1 001a100ea2 001a200ea3 001a300ea7
001a400eae 001a500eb1 ffffffffff 0000000010
000e000020 000be00030 0014d000df 00173000e0
00146000e1 0006300100 0008500200 000a200300
0002f00400 0003e00500 0004b00600 0005800700
000ef00800 007ce00900 0013300a00 0019700e00
001a600f00 0014000fc8 000e5a0001 000eaa0002
ffffffffff 0000000010 0002f00400 0003e00500
0004b00600 0005800700 0006300100 0008500200
000a200300 000be00030 000e000020 000e5a0001
000eaa0002 000ef00800 0013300a00 0014000fc8
00146000e1 0014d000df 00173000e0 0019700e00
001a600f00 007ce00900 ffffffffff ffffffffff
0000400004 ffffffffff
```

Code

```
241355f139 241a05f13b 241a05f13c 240034302f
4010f40117 2400543058 24006430be 407cf40000
407ee407ee 2413b201a0 5f13b24139 221a05f139
4a003240ef 5f13f24197 5f7ce2400e 2019f5f00e
2413f221a0 5f13f4800d 241a05f13b 241a15f13c
241355f139 240154303e 2401643058 24017430be
407cf40000 407ee407ee 2413b201a0 5f13b24139
221a05f139 4a015240ef 5f13f24197 5f7ce2401f
2019f5f01f 2413f221a0 5f13f4801e 241a05f13b
241a25f13c 241355f139 240264304b 2402743058
24028430be 407cf40000 407ee407ee 2413b201a0
5f13b24139 221a05f139 4a02600000 2019f54031
2019f5403d 2402f54035 5403651035 241a35f12d
2419e5f129 6010f38117 5f10f20129 5f12924035
201a55f035 240362019f 5f0362412d 221a05f12d
4a0354002f 4302f00000 2019f5404a 2419e5f129
6011f3811a 5f11f60120 3811b5f120 601213811c
5f12160122 3811d5f122 601233811e 5f12320122
2012120120 2011f5f129 4303e00000 2019f54057
2419e5f129 601243811a 5f12460125 3811b5f125
601263811c 5f12660127 3811d5f127 601283811e
5f12820127 2012620125 201245f129 4304b00000
2019f54062 241345f138 241335f137 2405b43063
2405c43085 24137221a0 5f1374a05b 2405f430a2
24138221a0 5f1384a05a 4305800000 2019f54084
```

240ef5f12c 60129380f0 5f12a600f1 387cf207d0
180103a0f2 7f12b2412b 2012a5f7de 601011b008
387d01b008 207cf207d1 180103a0f3 7f7df60102
1b008387d1 1b008207d0 207d218010 3a0f47f7e0
601031b008 387d21b008 207d1207d3 180103a0f5
7f7e160104 1b008387d3 1b008207d2 207d418010
3a0f67f7e2 7f7d3247e1 5f7d2247e0 5f7d1247df
5f7d0247de 5f7cf2412c 221a05f12c 4a06540063
4306300000 2019f540a1 601051b008 387d41b008
207d3207d5 180103a0f7 7f7e360106 1b008387d5
1b008207d4 207d618010 3a0f87f7e4 601071b008
387d61b008 207d5207d7 180103a0f9 7f7e560108
1b008387d7 1b008207d6 207d818010 3a0fa7f7e6
601091b008 387d81b008 207d7207d9 180103a0fb
7f7d8247e6 5f7d7247e5 5f7d6247e4 5f7d5247e3
5f7d440085 4308500000 2019f540bd 6010a1b008
387d91b008 207d8207da 180103a0fc 7f7e86010b
1b008387da 1b008207d9 207db18010 3a0fd7f7e9
6010c1b008 387db1b008 207da207dc 180103a0fe
7f7ea6010d 1b008387dc 1b008207db 207dd18010
3a0ff7f7eb 6010e1b008 387dd1b008 207dc18010
3a1007f7dd 247eb5f7dc 247ea5f7db 247e95f7da
247e85f7d9 430a200000 2019f540c1 2019f540c2
2019f540de 240be540cf 240be540d0 510d2400be
240c4430e0 400e500000 2413c12020 5f1318c131
240c8430e0 400ea00000 2413b12020 5f1328c132
8c0df430cd 241a15f13d 241a45f13e 607cf38136

5f7ee400be 240d143146 000648c7ee 240cf2019f

5f0cf240d0 2019f5f0d0 240d2201a0 5f0d22413d

221a05f13d 480db8c0df 410da241a1 5f13d2413e

221a05f13e 4a0cf400be 430be00000 3500000000

2019f540e2 2019f540e4 240e0540e3 880e0430e4

430e000000 3212340e0a 1e10321134 0e180e1c0a

1e13191810 3800000000 342d321e34 13170e1032

1334180c1c 0e170e181e 1038000000 0000000031

0b1c432ca5 2bc6a7ef9d 0000abc605 00026871fb

00054665ea 000b8f5bb9 001950a4ef 00011be76f

00026eb84d 00055332fa 000ba7af6d 001987ae93

00023ccca0 0004e6c8e6 000abc2887 001783d75c

00337ebb24 0001687339 0004466728 000a8f5cf7

001850a407 00001be687 00016eb765 0004533438

000aa7ae85 001887afd1 00013ccbb8 0003e6c7fe

0009bc29c4 001683d89a 00327ec2d3 0000e00041

0001b479de 0007466594 005ad3376c 000683d6fe

00022666d8 000a3852ac 0006a7af31 2ac083126e

3083126e97 36e978d4fd 7020c49ba5 7353f7ced9

7b22d0e560 7f8c0053e2 7f9db22d0e 0011547bad

0001c51e7a 000163d61b 000a8000ec 0006f47b67

000030a31c 00000ccddc 00004e14c7 00074ccc1c

0004ce148f 0000000000 0000000000 0000000000

0000000000 0000000000 0000000000 0000000000

0000000000 0000000000 0000000000 0000000018

0000000001 000000000e 53e2d6238d 0000000000

0000000000 0000000000 0000000000 0000000000

0000000000 0000000000 0000000000 0000000000

2414141141 2019f14014 51144941a6 1b03c54145

160094b19f 94fff41142 201a554148 201a554167

241465f14b 120145414c 2414a43173 0000000000

601464314e 201a554167 7f1a62416b 5e16224170

5f1a84a152 2416d41152 2416e5c164 251a620172

5f1a74e157 160007f1a7 6019841157 160007819d

241a64b15a 8c19a4115a 8c19c2416c 5c1628c19d

241a8201a0 5f1a84a164 241a71c002 201a718004

5819d1b008 100015f1a7 2719d4b158 8c1994315c

2416c52162 2416e5c164 4315e8c199 4314d26171

5f1a848166 2416f5c164 8c19b4315e 2719d4b14d

4115b4314d 2416c00000 4116700000 4116600000

0000000000 0000000009 0000000113 201a554175

201a554188 241735215b 5216612008 1e0047f1a9

1e0047f1aa 1e0047f171 581595815a 5816a58163

271a94b17e 241894117e 2418754159 261aa201a0

5f1704b182 2418841182 2417b51154 241aa20171

2018951185 2218a60173 4918716000 4019a7f172

4317340157 401994018a 4019940197 4000000000

0666666666 00a3d70a3d 0010624dd3 0001a36e2f

000029f16b 00000431be 0000006b60 0000000abd

0000000113 000000001b 0000000003 0000000000

0100000000 1000000000 2b00000000 2c00000000

2d00000000 0000000000 0000000000 0000100000

0000000001 0000000002 0000000003 0000000007

000000000e 0000100001 0000000fff 0000000000

0000000000 0000000000 0000000000 0000000000

0000000000 0000000000 0000000000 0000000000

THIS PAGE

WAS INTENTIONALLY

LEFT BLANK

ORNL-2812
Health and Safety
TID-4500 (15th ed.)

INTERNAL DISTRIBUTION

1. C. E. Center
2. Biology Library
3. Health Physics Library
4-5. Central Research Library
6. Reactor Experimental Engineering Library
7-26. Laboratory Records Department
27. Laboratory Records, ORNL R.C.
28. A. M. Weinberg
29. L. B. Emlet (K-25)
30. J. P. Murray (Y-12)
31. J. A. Swartout
32. E. H. Taylor
33. E. D. Shipley
34-35. F. L. Culler
36. M. L. Nelson
37. W. H. Jordan
38. C. P. Keim
39. J. H. Frye, Jr.
40. S. C. Lind
41. A. H. Snell
42. A. Hollaender
43. K. Z. Morgan
44. M. T. Kelley
45. T. A. Lincoln
46. R. S. Livingston
47. A. S. Householder
48. C. S. Harrill
49. C. E. Winters
50. H. E. Seagren
51. D. Phillips
52. W. K. Eister
53. F. R. Bruce
54. D. E. Ferguson
55. R. B. Lindauer
56. H. E. Goeller
57. C. W. Hancher
58. R. A. Charpie
59. J. A. Lane
60. M. J. Skinner
61. R. E. Blanco
62. G. E. Boyd
63. W. E. Unger
64. J. J. Perona
65. A. T. Gresky
66. E. D. Arnold
67. C. E. Guthrie
68. J. W. Ullmann
69. K. B. Brown (Y-12)
70. K. O. Johnsson
71. J. C. Bresee
72. P. M. Reyling
73. R. G. Wymer
74. J. O. Blomeke
75. W. J. Boegly
76. L. L. Ennis
77. H. W. Godbee
78. P. A. Haas
79. F. E. Harrington
80. R. W. Horton
81. E. Lamb
82. J. T. Long
83. F. L. Parker
84. J. T. Roberts
85. A. D. Ryon
86. E. G. Struxness
87. C. D. Watson
88-91. M. E. Whatley
92. D. L. Katz (consultant)
93. I. Perlman (consultant)
94. M. Benedict (consultant)
95. C. E. Larson (consultant)
96. H. Worthington (consultant)
97. J. H. Rushton (consultant)
98. ORNL - Y-12 Technical Library, Document Reference Section

EXTERNAL DISTRIBUTION

99. Division of Research and Development, AEC, ORO
100-101. AEC, Washington (1 copy each to W. G. Belter and J. A. Lieberman)
102-103. Brookhaven National Laboratory (1 copy each to L.P. Hatch and B. Manowitz)
104. Phillips Petroleum Company (C. E. Stevenson)

105. Hanford Atomic Products Operation (L. P. Bupp)
106. Savannah River Operations Office (J. W. Morris)
107. Argonne National Laboratory (S. Lawroski)
108-738. Given distribution as shown in TID-4500 (15th ed.) under Health and Safety category (100 copies - OTS)